JOURNAL OF GEOPHYSICAL RESEARCH, VOL. 103, NO. B6, PAGES 12,181–12,203, JUNE 10, 1998

Estimation of current plate motions in Papua New Guinea from Global Positioning System observations

Paul Tregoning,[1] Kurt Lambeck,[1] Art Stolz,[2] Peter Morgan,[3] Simon C. McClusky,[4] Peter van der Beek,[1] Herbert McQueen,[1] Russell J. Jackson,[5] Rodney P. Little,[5] Alex Laing,[6,7] and Brian Murphy[8]

Abstract. Plate tectonic motions have been estimated in Papua New Guinea from a 20 station network of Global Positioning System sites that has been observed over five campaigns from 1990 to 1996. The present velocities of the sites are consistent with geological models in which the South Bismarck, Woodlark, and Solomon Sea Plates form the principal tectonic elements between the Pacific and Australian Plates in this region. Active spreading is observed on the Woodlark Basin Spreading Centre but at a rate that is about half the rate determined from magnetic reversals. The other major motions observed are subduction on the New Britain Trench, seafloor spreading across the Bismarck Sea Seismic Lineation, convergence across the Ramu-Markham Fault and left-lateral strike slip across the Papuan Peninsula. These motions are consistent with a 8.2° Myr^{-1} clockwise rotation of the South Bismarck Plate about a pole in the Huon Gulf and a rotation of the Woodlark Plate away from the Australian Plate. Second order deformation may also be occurring; in particular, Manus Island and northern New Ireland may be moving northward relative to the Pacific Plate at ~5-8 mm yr^{-1} (significant at the 95% but not at the 99% confidence level) which may suggest the existence of a North Bismarck Plate.

1. Introduction

Papua New Guinea (PNG) is a complex tectonic region at the convergence of the Australian and Pacific Plates. Up to four minor plates may be trapped in this collision in response to the convergence of the two major plates (Figure 1). PNG is also a region of active and dormant volcanoes and of intense and frequent earthquake activity at all depths. At least seven plate tectonic models based on geology and seismicity have been proposed for the region [e.g., *Johnson and Molnar*, 1972; *Curtis*, 1973; *Krause*, 1973; *Hamilton*, 1979; *Davies et al.*, 1984; *Taylor et al.*, 1991]. Whilst these models have similarities, they also exhibit considerable differences including the number and location of minor plates. This leaves many questions about the location of plate margins and the sense of motion unresolved. For example, how many minor plates are there? Is there a North Bismarck Plate as proposed by *Johnson and Molnar* [1972]? Where is the active boundary between the Australian and South Bismarck Plates? Where are the poles of rotation of the minor plates? Do present-day motions agree with those determined from the geological record?

Geodetic observations provide the means to answer these questions by measuring crustal motions and deformation over time intervals of a few years or less. It then becomes possible to define the present-day kinematics of plate motions independent of geological data. The Global Positioning System (GPS) has proven to be a successful tool for the determination of plate tectonic motion and deformation [e.g., *Feigl et al.*, 1993; *Robbins et al.*, 1993; *McClusky et al.*, 1994; *Larson et al.*, 1997; *Tregoning et al.*, 1994; *Argus and Heflin*, 1995]. In this paper we present plate motions in the PNG region determined from GPS measurements. The sites were observed with GPS in four campaigns during 1990-1993 and again in 1996. The GPS data were analyzed using the GAMIT [*King and Bock*, 1996] and GLOBK [T.A. Herring, GLOBK global Kalman filter VLBI and GPS analysis program, version 4.1, Mass. Inst. of Technol., Cambridge, 1997, hereinafter referred to as T.A. Herring, 1997] software.

Below we review the tectonics of this complex region. We then describe the GPS surveys and our data analysis procedures. Next we present the site velocities determined by GPS and compute Euler poles of rotation of the minor plates. Finally, we give a tectonic interpretation of these motions. The results provide answers to some of the above questions by establishing the kinematic pattern of the principal plate motions and crustal deformation of the region.

2. Plate Configurations and Motions in Papua New Guinea

Papua New Guinea lies within one of the more complex tectonic regions of the world. Active plate boundaries have

1 Research School of Earth Sciences, The Australian National University, Canberra, A.C.T., Australia.
2 School of Geomatic Engineering, The University of New Wales, Sydney, New South Wales, Australia.
3 School of Information Science and Engineering, University of Canberra, Canberra, A.C.T., Australia.
4 Department of Earth, Atmospheric and Planetary Sciences, Massachusetts Institute of Technology, Cambridge.
5 Department of Surveying and Land Studies, The Papua New Guinea University of Technology, Lae.
6 National Mapping Bureau, Port Moresby, Papua New Guinea.
7 Deceased October 20, 1997.
8 Australian Surveying and Land Information Group, Canberra, A.C.T., Australia.

Paper number 97JB03676.
0148-0227/98/97JB-03676$09.00

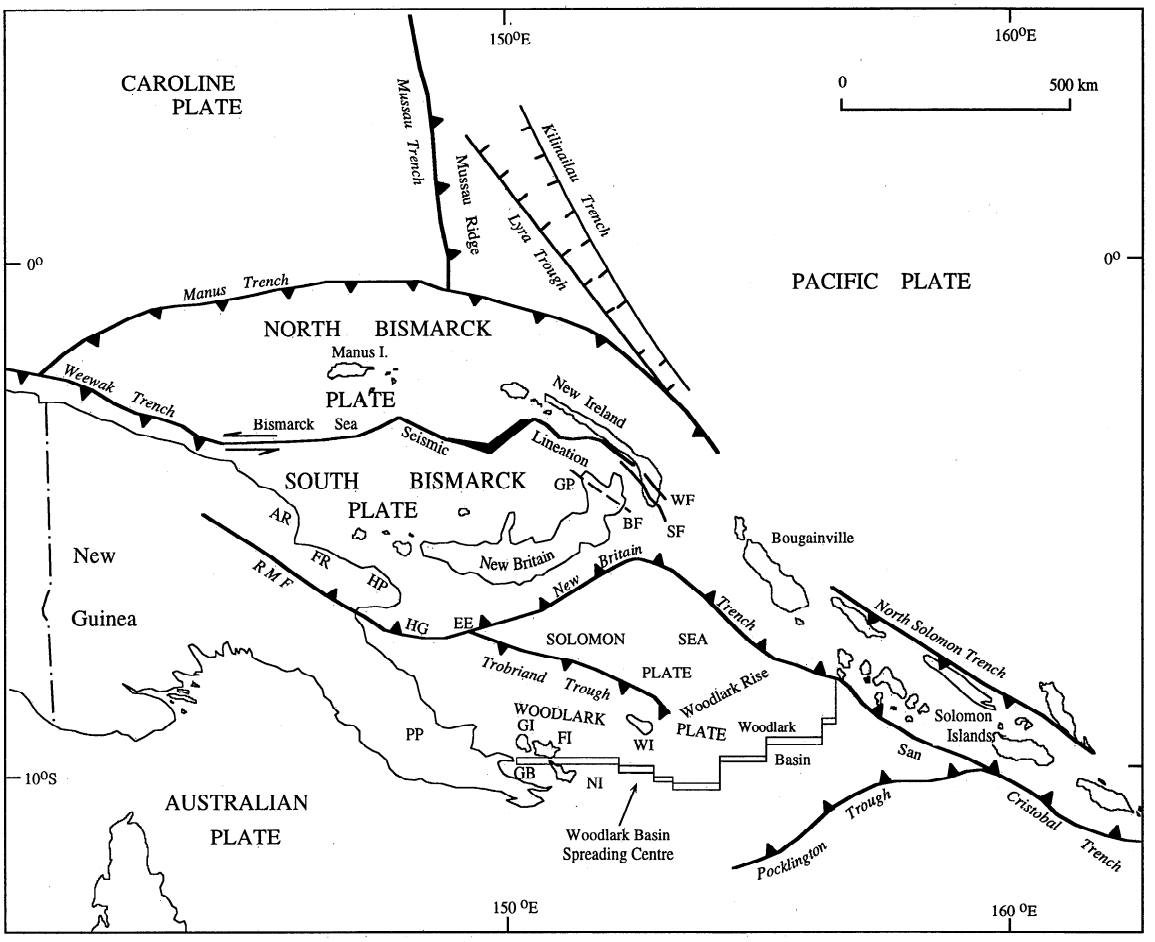

Figure 1. The map of Papua New Guinea (PNG) showing locations of major tectonic elements: AR, Adelbert Range; BF, Baining Fault; EE, 149°E Embayment; FI, Fergusson Island; FR, Finisterre Range; GB, Goodenough Bay; GI, Goodenough Island; GP, Gazelle Peninsula; HG, Huon Gulf; HP, Huon Peninsula; NI, Normanby Island; PP, Papuan Peninsula; RMF, Ramu-Markham Fault; SF, Sapom Fault; WF, Weitin Fault; and WI, Woodlark Island.

been defined on the basis of information from earthquake-epicentre distribution and seafloor morphology, and the locations of some of these boundaries are undisputed. From its junction with the Trobriand Trough at ~149°E the boundary between the Solomon Sea and South Bismarck Plates follows the axis of the New Britain Trench east to where the trench meets the San Cristobal Trench, southwest of Bougainville (Figure 1). The northern margin of the South Bismarck Plate in the Manus Basin coincides with a spreading transform system that is well defined by both the earthquake-epicentre locations and seafloor morphology [*Taylor*, 1979; *Eguchi et al.*, 1989]. The boundary between the Australian Plate and the oceanic seafloor north of it is the Woodlark Basin Spreading Centre. Other plate boundaries are not so clearly defined.

A number of different plate configurations have been proposed (Figure 2). All models include at least two minor plates between the Australian and Pacific Plates: the South Bismarck and Solomon Sea Plates. *Johnson and Molnar* [1972] introduced a third plate, the North Bismarck Plate (Figure 2a), which then featured in a number of the other models. *Hamilton* [1979] and *Davies et al.* [1984] proposed a fourth plate, the Woodlark Plate, located in the Woodlark Basin of the Solomon Sea (Figures 2e and 2f), while *Davies et al.* [1984] speculated on the existence of a fifth plate, the Trobriand Plate, situated east of the Papuan Peninsula (Figure 2f). These models suggest a plate configuration that could include some or all of the following plates in addition to the Pacific and Australian Plates: Caroline, North Bismarck, South Bismarck, Solomon Sea, Trobriand, and Woodlark Plates (Figures 1 and 2). Below we examine the geological information relating to the boundaries of these plates and the geological features comprising the Papua New Guinea region, emphasizing those aspects that may be relevant to the interpretation of the geodetic data.

Figure 2. The plate configurations for PNG proposed by different authors: (a) adapted *from Johnson and Molnar* [1972]; (b) adapted from *Curtis* [1973]; (c) adapted from *Krause* [1973]; (d) adapted from *Taylor* [1975]; (e) adapted from *Hamilton* [1979]; (f) adapted from *Davies et al.* [1984]; (g) adapted from *Taylor et al.* [1991]; (h) a priori model of this paper.

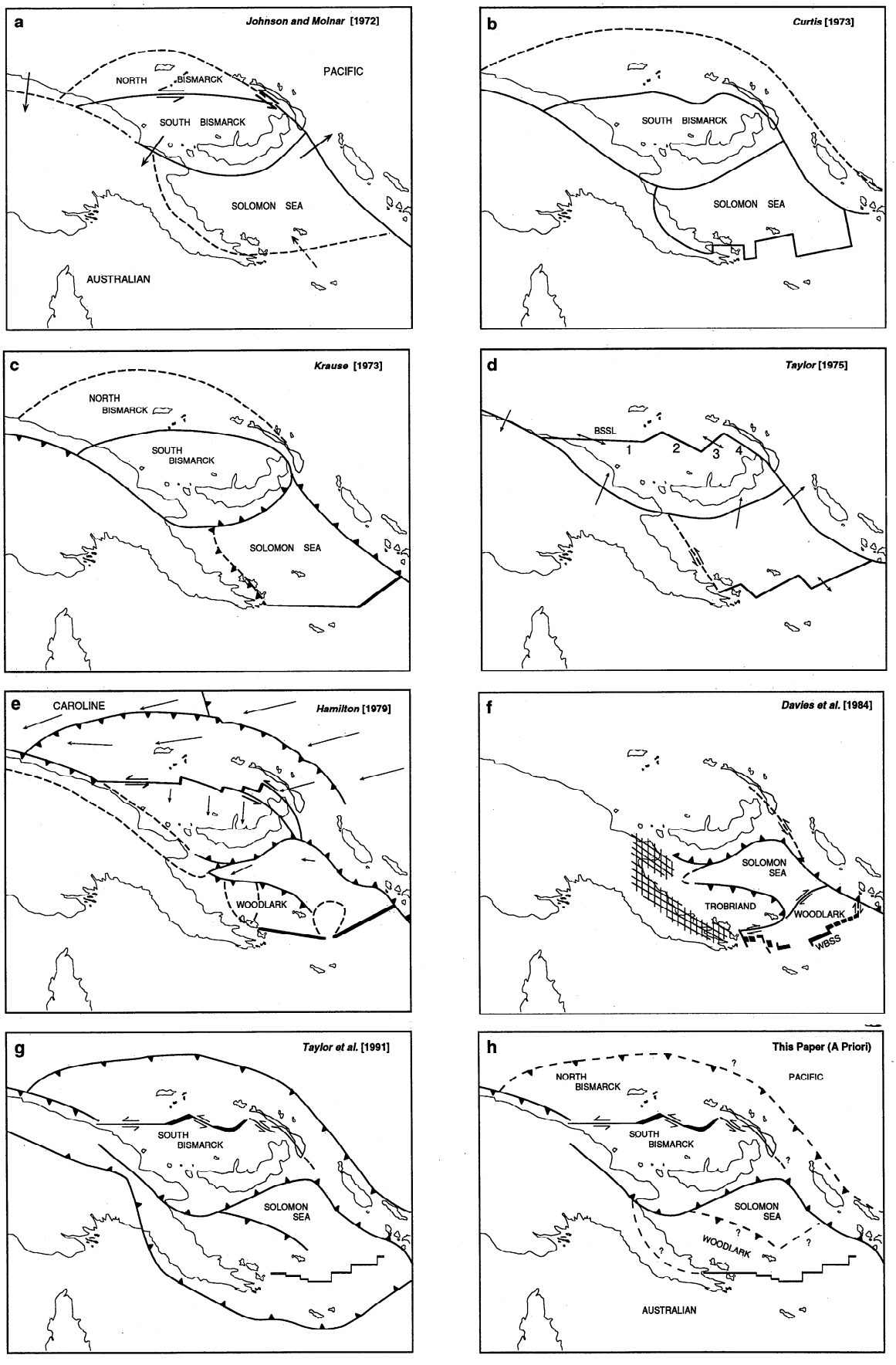
a
Johnson and Molnar [1972]
NORTH BISMARCK
PACIFIC
SOUTH BISMARCK
SOLOMON SEA
AUSTRALIAN
b
Curtis [1973]
SOUTH BISMARCK
SOLOMON SEA
c
Krause [1973]
NORTH BISMARCK
SOUTH BISMARCK
SOLOMON SEA
d
Taylor [1975]
BSSL
1
2
3
4
e
CAROLINE
Hamilton [1979]
WOODLARK
f
Davies et al. [1984]
SOLOMON SEA
TROBRIAND
WOODLARK
WBSS
g
Taylor et al. [1991]
SOUTH BISMARCK
SOLOMON SEA
h
This Paper (A Priori)
NORTH BISMARCK
PACIFIC
SOUTH BISMARCK
SOLOMON SEA
WOODLARK
AUSTRALIAN

2.1. Caroline Plate

There has been some conjecture as to whether there is a separate Caroline Plate located between the Pacific Plate and the Phillipine Sea Plate. *Weissel and Anderson* [1978] concluded that there is such a plate extending southward to the Manus Trench and, on the basis of plate motion reconstructions, considered the Manus and Mussau Trenches to be active plate boundaries. *Hegarty et al.* [1983] and *Ryan and Marlow* [1988] stated that the Caroline Plate is underthrusting the Pacific Plate along the southern part of the Mussau Trench. In contrast, on the basis of earthquake fault plane solutions, *McCaffrey* [1996] inferred that the Caroline/Pacific plate boundary may just be a region of stress concentration due to the geometry of the plates and concluded that the motion of a supposed Caroline Plate is indistinguishable from that of the Pacific Plate. There is also little seismic activity along this boundary. *Erlandson et al.* [1976] interpreted the Mussau Ridge as an overthrust segment of crust and stated that there are no Benioff zones. *Johnson* [1979] stated that the Manus and Mussau Trenches are relatively young features and barely active, possibly so young that subduction occurs incipiently.

2.2. North Bismarck Plate

Johnson and Molnar [1972] proposed a North Bismarck Plate, located between the South Bismarck Plate and the Pacific Plate. The northern boundary of this plate is considered to correspond to the Manus Trench extending arcuately from the Wewak Trench in the west to the Lyra Trough in the east (Figure 1) with the southern boundary being the Bismarck Sea Seismic Lineation.

The Manus Trench appears to have trench wall features that are characteristic of an active subduction zone [*Ryan and Marlow*, 1988]. However, it lacks the significant seismicity and arc-type volcanism that is characteristic of rapid convergence and subduction [*Johnson and Molnar*, 1972]. Additional data is needed, particularly along the western segment of the Manus Trench, to determine whether the trench now forms an active plate boundary and whether there is a need to introduce the North Bismarck Plate in the present-day plate models. In the absence of conclusive evidence for such a boundary, it is possible that the Bismarck Sea Seismic Lineation forms the southern boundary of the Pacific Plate.

2.3. Bismarck Sea Seismic Lineation

The northern margin of the South Bismarck Plate is defined by a band of seismicity, named the Bismarck Sea Seismic Lineation by *Denham* [1969], which extends from a point near the northeastern tip of New Britain in the east to the north coast of New Guinea in the west. The predominant focal mechanism of this seismicity is strike-slip. *Taylor* [1975, 1979] divided the lineation into four main geographical sections, each being associated with a separate transform fault segment (Figure 2d). Motion on these transform faults is recognized as being left-lateral. On the westernmost section (1 in Figure 2d) the fault planes are oriented east-west. This trend continues onto the land in a series of anastomosing faults that cut westward through the Toricelli and Bewani Mountains of northern New Guinea [*Cooper and Taylor*, 1987a]. Focal mechanisms for the second section, marked by a prominent ridge and scarp [*Taylor*, 1979], indicate fault planes that are oriented northwest-southeast. The third section, a northeast-southwest trending section, is actively spreading. Magnetic anomaly data indicate that the spreading rate is in excess of 100 mm yr^{-1} [*Martinez and Taylor*, 1993]. The fourth and easternmost section also trends northwest-southeast. The surface expressions of this boundary are the Baining, Sapom, and Weitin Faults in the Gazelle Peninsula and New Ireland [*D'Addario et al.*, 1976] (Figure 1).

2.4. Eastern Margin of the South Bismarck-Pacific Plate Boundary

The seismically active Weitin Fault [*Hamilton*, 1979; *Mori*, 1989] has been interpreted as forming the eastern margin of the South Bismarck Plate. *Mori* [1989] described an $Ms = 7.2$ northeast dipping thrust earthquake which occurred in 1985 in this region. Aftershock locations (mainly left-lateral strike-slip) indicate a rupture ~50 km long in a northwest-southeast direction. The thrust focal mechanism of the main event is not consistent with the left-lateral transform boundary of the plate, and so, the seismicity of the area may be indicative of a more complex tectonic structure [*Mori*, 1989]. Beyond the southern tip of New Ireland the location of this boundary is uncertain [*Davies et al.*, 1984; *Eguchi et al.*, 1989; *Taylor et al.*, 1991].

2.5. New Britain Trench

The New Britain Trench forms the northern margin of the Solomon Sea Plate. It extends from its junction with the Trobriand Trough and the seaward extension of the Ramu-Markham Fault in the west at the 149° Embayment [*Davies et al.*, 1984] to the triple junction with the San Cristobal Trench and the Woodlark Basin Spreading Centre in the east [Taylor, 1987] (Figure 1). It is characterized by its abrupt termination at the 149° Embayment and by the 70° southward bend at ~153°E and is associated with a high level of seismicity as illustrated in Figure 3 [*Engdahl et al.*, 1998; *Cooper and Taylor*, 1987a,b]. Fault plane solutions indicate that convergence occurs in a direction that is generally normal to the trench axis. Estimates of convergence at the trench vary between 92 and 125 mm yr^{-1} [*Johnson*, 1979].

2.6. Trobriand Trough

Hamilton [1979] suggested from the trench-like appearance of the Trobriand Trough that the Solomon Sea lithosphere subducts beneath the Trobriand Platform. *Davies et al.* [1984] suggested that this trough is currently active or has recently been active on the basis of the occurrence of Pliocene-Quaternary arc-trench volcanism on the Papuan Peninsula as well as seismic reflection data. More recently, *Pegler et al.* [1995] showed that the seismicity distribution beneath the Papuan Peninsula is consistent with a southward dipping Benioff zone. Data discussed by *Davies et al.* [1987] and *Lock et al.* [1987] indicate that the Trobriand Trough is filled with a thick southward dipping sediment sequence. On the inner trench wall this sequence is deformed by thrust faults, whereas on the outer wall normal faults dominate, indicative of geologically recent subduction. Only the youngest sediments onlap the frontal anticline of the inner trench wall, possibly indicating that the subduction has recently ceased. If subduction is occurring, estimates of the rate are between 6 [*Kirchoff-Stein*, 1992] and 20 mm yr^{-1} [*Eiichi et al.*, 1986]. Because there is no land on the Solomon Sea Plate north of the Trobriand Trough, no geodetic estimate of convergence across this trough is possible, and we cannot establish whether or not this trough forms an active margin for the Solomon Sea Plate.

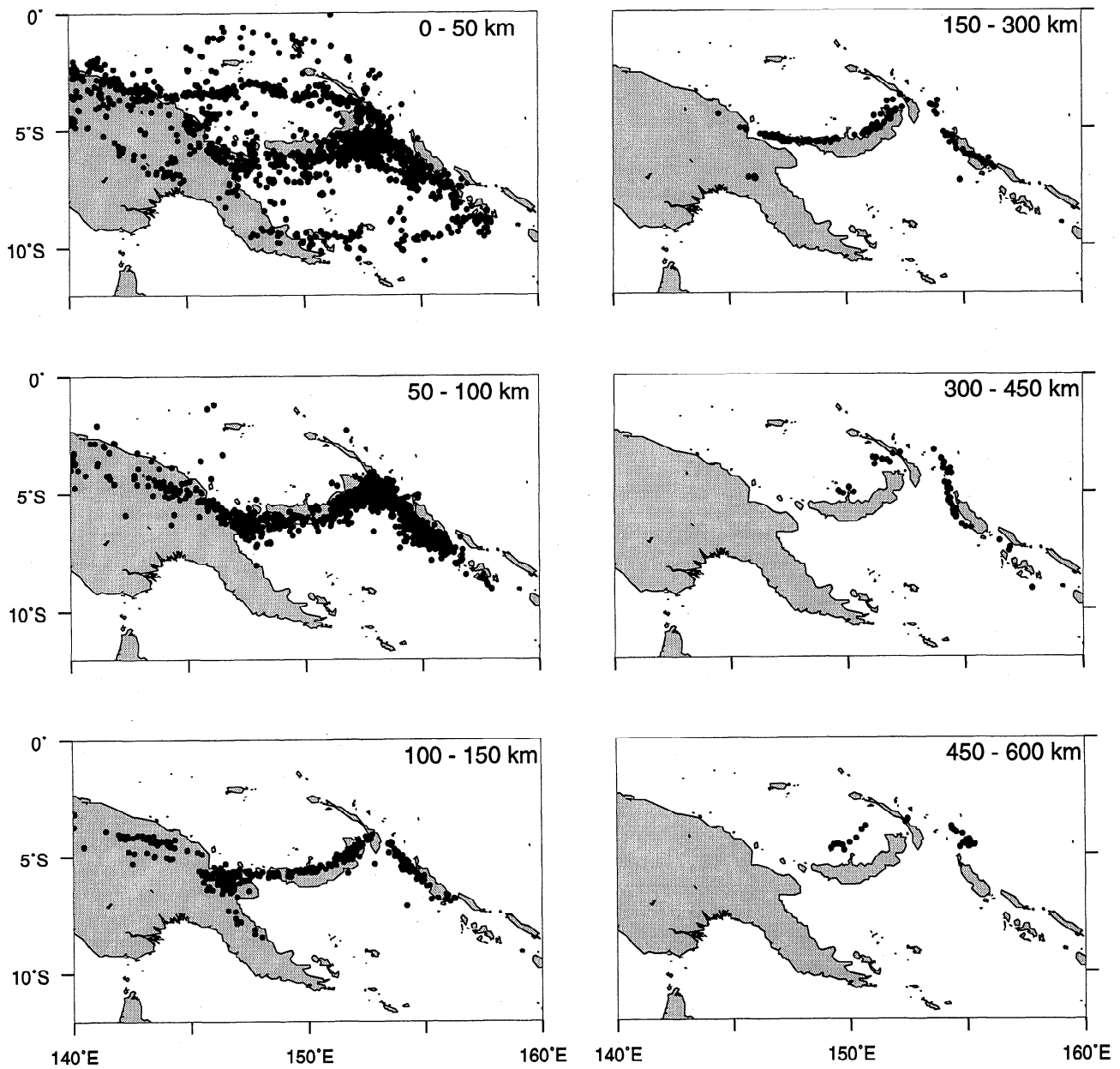

Figure 3. The seismicity of the PNG region 1964-1994. Relocated earthquake events from *Engdahl et al.* [1998].

2.7. Woodlark Basin

The Woodlark Basin is bounded on the northeast by the Solomon Island arc, on the northwest by the Woodlark Rise, and on the southeast by the Pocklington Trough. The main features of the basin are the two topographic rises, the Woodlark Rise in the north and the Pocklington Rise in the south, separated by an active spreading zone, the Woodlark Basin Spreading Centre. Shallow earthquakes define a zone of weak activity along the northern flank of the Woodlark Rise which has been used to argue for a plate boundary between a Woodlark Plate and the Solomon Sea Plate [*Davies et al.*, 1984] (Figure 2f). However, this interpretation is based on the fault mechanism of a single right-lateral strike-slip earthquake [*Weissel et al.*, 1982] and so lacks substantial evidence.

In the eastern Woodlark Basin, seafloor spreading is characterized by east-west trending rift segments offset by north-south transforms [*Taylor*, 1987]. The spreading center is represented by an axial rift valley, whose width and height decrease from east to west [*Taylor and Exon*, 1987]. Seismic reflection data and magnetic anomalies clearly define the spreading axis between 151°40'E and 157°E [*Benes et al.*, 1994]. From magnetic reversals, *Benes et al.* [1994] estimated the half-spreading rate at 153°29.4'E and 152°30'E to be 26 and 20 mm yr^{-1}, respectively. They calculated the relative pole of rotation of the Solomon Sea Plate with respect to the Australian Plate to be 9°30'S, 148°56'E with a rate of rotation of 5.6° Myr^{-1}. Spreading is occurring faster on the northern side than on the southern side of the ridge [*Weissel et al.*, 1982]. From a 1993 geophysical and sidescan sonar survey, *Goodliffe et al.* [1997] concluded that the spreading center axis jumped (rather than propagated) to a new location at ~80 ka. This implies that any pole of rotation estimated from magnetic

reversal chronology will not necessarily represent the present-day motions.

West of 151°E, the rift becomes less distinct. Between the Papuan Peninsula and the D'Entrecasteaux Islands, the boundary appears as a series of horst blocks and sediment-filled grabens that are indicative of divergence. A diffuse zone of shallow earthquakes trends westward between Fergusson and Normanby Islands, and there is petrologic evidence which suggests that rifting may be occurring there [*Smith*, 1976]. The cores of the D'Entrecasteaux Islands themselves are active metamorphic core complexes [*Baldwin et al.*, 1993] indicative of rapid divergence over the past 4 Myr. A further zone of earthquakes, exhibiting mainly tensional focal mechanisms, extends west into Goodenough Bay, the Papuan Peninsula [*Ripper*, 1982; *Davies et al.*, 1984] (Figure 3) and as far west as 148°E [*Taylor et al.*, 1995], indicating that the plate boundary extends at least that far to the west.

2.8. Australian and South Bismarck Plate Boundary

The Australian and South Bismarck Plates are in collisional contact along the Ramu-Markham Fault [*Johnson*, 1979]. On the basis of the closure of South Bismarck, Pacific, and Australian Plate Euler vectors, *Taylor* [1979] estimated the relative motion between the Australian and South Bismarck Plates at 144°E to be 65 mm yr^{-1} in a northeasterly direction. However, *Johnson* [1979] indicated that the Taylor closure of plate vectors may not be accurate, thereby invalidating this estimate of the relative motion between these two plates.

Pegler et al. [1995] identified an inverted U-shaped zone of seismicity beneath the Finisterre Range and the New Guinea Highlands which they interpreted as a wedge of doubly subducting Solomon Sea Plate lithosphere. This supported the conclusions of *Ripper* [1982], *Davies et al.* [1984], and *Cooper and Taylor* [1987a] that the southward dipping slab beneath the eastern part of New Guinea is a remnant of the Solomon Sea Plate slab which has been subducted at the Trobriand Trough. It has been proposed [e.g., *Dewey and Bird*, 1970; *Karig*, 1972; *Hamilton*, 1973; *Cooper and Taylor*, 1987a] that subduction reversal occurred in this region, thereby explaining the existence of both northward and southward dipping slabs beneath the Papuan and Huon Peninsulas. *Johnson and Jaques* [1980] claimed that there was no convincing seismic evidence for a southward dipping slab and no bathymetric evidence for an active submarine trench north of the Huon Peninsula. They believed that polarity reversal had not occurred but that the subducting Australian lithosphere became vertically suspended as a result of the continent-arc collision. *Abbott* [1995] claimed that there was no southward subduction as there is evidence of sediments from the Australian Plate in accretionary wedges in the Adelbert and Finisterre Ranges to the north of the Ramu-Markham Fault, indicating that in the past the Australian Plate had subducted beneath these ranges.

Between longitudes of ~144°E and 148°E, both the distribution of seismicity and the earthquake focal mechanisms indicate that convergence is accommodated by thrusting of the continental crust. Much of the deformation seems to be taken up on the Ramu-Markham Fault which in the Finisterre Range appears to form a north dipping thrust along which the Finisterre block overrides the New Guinea mainland [*Abers and Roecker*, 1991; *Pegler et al.*, 1995; C. Stevens et al., Low-angle, mid-crustal detachment and ramp faulting in the Markham valley, submitted to Geology, 1998, hereinafter referred to as C. Stevens et al., 1998].

2.9. A Priori Plate Model

From the available geophysical information it appears that the convergence of the Australian and Pacific Plates might be accommodated by up to four microplates: North Bismarck, South Bismarck, Solomon Sea, and Woodlark (Figure 2h). Without geodetic data from sites located on either the Caroline Plate or the Solomon Sea Plate we cannot resolve the questions surrounding the existence of the Caroline Plate nor whether the Solomon Sea Plate is being actively subducted at the Trobriand Trough.

Whether a Caroline Plate exists or not has no effect on our results, so we refer to all lithosphere north of the Manus Trench as the Pacific Plate. The available geophysical evidence indicates that at least in the recent past the Solomon Sea and the Woodlark plates were different blocks, hence our adoption of the Woodlark Plate in our a priori model.

3. GPS Crustal Motion Surveys in Papua New Guinea

A total of 20 stations have been observed with GPS since 1990 as part of a geodetic network designed to measure crustal deformation and to gain an understanding of the present-day large-scale tectonic motions. There have been earlier terrestrial geodetic surveys in PNG aimed at determining crustal motion in specific localities [e.g., *Sloane and Steed*, 1976], but little work has been done to establish the regional kinematic pattern. *McClusky et al.* [1994] made preliminary comparisons between baseline lengths derived from Doppler and GPS, and C. Stevens et al. (1998) have used GPS to monitor deformation on the Ramu-Markham Fault. *Mobbs* [1997] determined preliminary velocities for some sites in PNG, but the analysis was limited by the large uncertainties of the estimates due to a short time interval between occupations of the sites. The analysis in this paper is based on five GPS surveys during 1990-1993 and 1996. The network configurations varied in the surveys conducted from 1990 to 1993, whilst in 1996 we occupied simultaneously a total of 15 of the previously observed sites including all of the sites initially observed in 1990. Five sites which were observed in the D'Entrecasteaux Islands in 1991 have not yet been reoccupied and will not be discussed in this paper.

There are three locations in PNG where there have been observations taken on more than one mark at the same location: Alotau, Misima, and Guasopa. The station observed at Alotau in 1990 was abandoned because of concerns of local stability, and a new mark was used in subsequent occupations. Two marks have been occupied at the other two sites as a result of operator confusion. Both terrestrial and GPS site ties exist between the local marks; however, because the sites have been occupied on two or more occasions, they have been analyzed here independently, thus providing a check on the accuracy of the velocity estimates.

The GPS observations were made with a mixture of receiver types (Trimble: 4000 SDT, 4000 SST, 4000 SSE and 4000 SSI and Ashtech: PXII and ZXII), and the duration of observations varied from 12 to 24 hours per day. In addition, the global GPS tracking network evolved considerably from just 13 sites in

Table 1. Site Names, Site Codes, Ground Mark Identification Numbers and Velocities and Associated (1σ) Standard Deviations in mm yr^{-1} Estimated from Global Positioning System (GPS) Observations

Site	Site Code	Survey Identifier	Latitude	Longitude	V_n	σv_n	V_e	σv_e
Alotau	ALT1	PM 9377	S10°18.8'	E150°27.4'	-	-	-	-
Alotau	ALT2	PM 9538	S10°18.6'	E150°20.3'	59.0	1.6	29.2	3.8
Carteret	CART	GS 9856	S04°47.0'	E155°27.8'	19.3	2.4	-61.2	4.6
Guasopa	GUA1	PM 9519	S09°13.5'	E152°56.6'	84.6	2.0	21.2	4.6
Guasopa	GUA2	AA 595	S09°13.5'	E152°56.6'	84.4	2.4	20.0	4.6
Jacquinot Bay	JACQ	PM 9515	S05°38.7'	E151°30.3'	-49.7	2.2	17.0	4.1
Kavieng	KAVI	PM 9513	S02°34.9'	E150°48.4'	32.6	1.6	-62.5	2.7
Lae (Unitech)	LAE1	LAE1	S06°40.4'	E146°59.6'	62.0	2.0	20.6	3.1
Losuia	LOUS	AA 583	S08°32.1'	E151°07.5'	76.0	1.4	22.1	2.5
Madang	MADA	AA 053	S05°09.7'	E145°44.9'	-	-	-	-
Madang	MAD1	PSM15495	S05°12.7'	E145°46.9'	39.9	2.0	24.2	3.1
Manus	MANU	Manus Secor 9522	S02°03.0'	E147°21.6'	28.2	1.8	-62.9	2.9
Misima Island	MISI	PM 9520	S10°41.3'	E152°50.0'	57.6	1.5	28.5	2.7
Misima Island	MIS1	PM 9195	S10°41.3'	E152°50.4'	56.9	2.0	26.2	3.1
Port Moresby	MORE	PSM15832	S09°26.0'	E147°11.2'	56.9	1.4	29.8	2.5
Morobe	MORO	PM 9517	S07°44.5'	E147°35.4'	63.9	1.8	27.1	2.9
Nuguria	NUGU	AA 619	S03°20.1'	E154°40.5'	19.3	2.4	-65.0	4.6
Rabaul	RABL	PSM23074	S04°11.5'	E152°09.7'	-98.3	2.4	22.0	4.6
Witu Island	WITU	PM 9516	S04°41.3'	E149°26.1'	-23.0	4.2	27.6	8.1
Lae (Unitech)	UNIT	PM 38	S06°40.3'	E146°59.9'	-	-	-	-

1990 to over 100 sites in 1996, while the number of satellites increased from 10 to 24. Consequently, the accuracy of the determination of the orbits of the satellites and hence the accuracy of the GPS solutions improved with time from 1990 to 1996. Table 1 lists the PNG sites which were observed, the actual survey mark identifier, and four character codes which will be used in this paper when referring to particular sites. Table 2 summarizes the history of the PNG site occupations throughout all the GPS surveys. The site locations are shown in Figure 6 (below). A full description of the 1990-1993 fieldwork is given by *McClusky et al.* [1994] and *Mobbs* [1997].

4. Results

The GPS data were processed with the GAMIT/GLOBK software [*King and Bock*, 1996; T.A. Herring, 1997] in a two-step procedure resulting in velocity estimates of the PNG sites in the International Terrestrial Reference Frame 94 (ITRF94) [*Boucher et al.*, 1996]. We define the terrestrial reference frame by transforming the coordinates and velocities of a free-network solution onto the coordinates of the 13 core sites of the International GPS Service for Geodynamics (IGS) network [*Mueller and Beutler*, 1992] (Figure 4). The analysis procedure is explained in detail in Appendix A. We found a misfit between the velocity fields of ITRF94 and the No-Net-Rotation-NUVEL-1A (NNR1A) global plate motion model [*DeMets et al.*, 1994] of 1-2 mm yr^{-1} and our results agree more closely with ITRF94 (see Appendix A).

In the following discussion our estimated velocities for the PNG sites relative to ITRF94 will be referred to as absolute velocities in order to distinguish them from the relative velocities of one plate with respect to another. In fact, it is impossible to measure a truly "absolute" velocity with GPS since there is a dependence of the GPS solution on an externally defined reference frame. However, since ITRF94 is a combination of different space geodetic solutions and the NNR1A absolute plate motion model (here again, we use the term absolute in the sense of "not relative"), we consider the estimated GPS site velocities to represent the motions of the sites with respect to the geocenter of the Earth and the three coordinate axes which define ITRF94.

4.1. Accuracy of GPS Velocity Estimates

The uncertainties of velocity estimates are as important as the estimates of the velocities themselves, but realistic estimates of the uncertainties are difficult to achieve. The computed quantities are the coordinates of the sites, and the velocity of a site may be inferred from the slope of a regression between all coordinate estimates of a site if we assume that the velocity at the site is constant. In reality the velocity estimates were computed from a deterministic Kalman

Table 2. Day-of-Year Occupations for the Papua New Guinea GPS Sites From 1990 to 1996

Site	1990	1991	1992	1993	1996
ALT2	-	222-232	-	244-245	240-247
CART	-	-	125-132	-	241-247
GUA1	215	231	-	-	240-248
GUA2	216-219	232		-	248[a]
JACQ	209-217	-	125-133	-	240-247
KAVI	211-214	-	125-133	150-154	240-247
				161-163	
LAE1	-	-	-	-	240-247[b]
LOUS	209-218	222-230	127-133	139-141	240-247
MAD1	-	-	-	240-245	240-247
MANU	209-213	-	-	247-248	240-247
MISI	215-219	221,222	-	134-138	240-243
		227,228			
MIS1	-	223-226	-	-	240
		229-232			244-247
MORE	209-219	222-224	125,126	134-146	240-248
		226	132,133	150-154	
				165,166	
				230-248	
MORO	209-219	-	-	144-146	240-247
NUGU	-	-	125-132	-	241-247
RABL	-	-	125-131	-	246-248
UNIT	-	-	-	243-245[b]	-
WITU	209-218	-	-	-	240-247

[a] GUA2 observed simultaneously with GUA1 for only 2 hours on day 248, 1996.
[b] Site UNIT was not occupied in 1996; a local tie was used to connect the UNIT and LAE1 sites.

filter solution in which the full covariance matrix was used. The velocity uncertainties are therefore a function of the accuracy of the coordinates at each epoch and the time interval between epochs [*Morgan*, 1994]. It is the former that is difficult to assess realistically. Usually, it will not suffice to adopt the formal variances and covariances resulting from each epoch solution since these will not reflect any unmodeled systematic errors such as antenna centering and the reference frame definition. Thus the resulting precision estimates are usually much smaller than the actual level of accuracy.

Experiments in which site velocities are estimated from long time series of coordinates indicate a scatter that exceeds the formal precision estimates and points to a need to scale the covariance matrices upward. *Feigl et al.* [1993] found it necessary to scale their covariance matrix upward by $\sim(2.2)^2$ and obtained velocity uncertainties of 1-5 mm yr^{-1} (1σ). Other investigators found that a simple scaling of the covariance matrix was inadequate and have suggested that the variances should be increased by a constant amount [e.g., *Hudnut et al.*, 1996] or by an amount that is a function of the duration of the experiment [e.g., *Argus and Heflin*, 1995; *Larson et al.*, 1998]. In all cases the resulting velocity uncertainties were of the order of 2-5 mm yr^{-1} (1σ).

In the present analysis the station coordinates and velocities were computed from a rigorous deterministic solution (Table 1), and the precisions of the coordinates for each epoch have been computed from the scatter of daily coordinates for each site in a back filter solution with stochastic estimation of the PNG site coordinates (Figure 5 and see Appendix A). This procedure is known to produce larger variances than the forward deterministic process since the daily correlation is decoupled by the stochastic modeling [see, e.g., *Tregoning*, 1996]. The precision of the velocities of the sites was then estimated from the weighted least squares fit of a linear trend through the coordinates (Figure 6). In most cases where there are three or more estimates of coordinates the regression line lies within the 1σ error bars, indicating that the coordinate uncertainties are realistic. In general, the (1σ) velocity uncertainties are ~2 mm yr^{-1} for the north components and 3-5 mm yr^{-1} for the east components (Table 1) in agreement with the results of other investigators as discussed above.

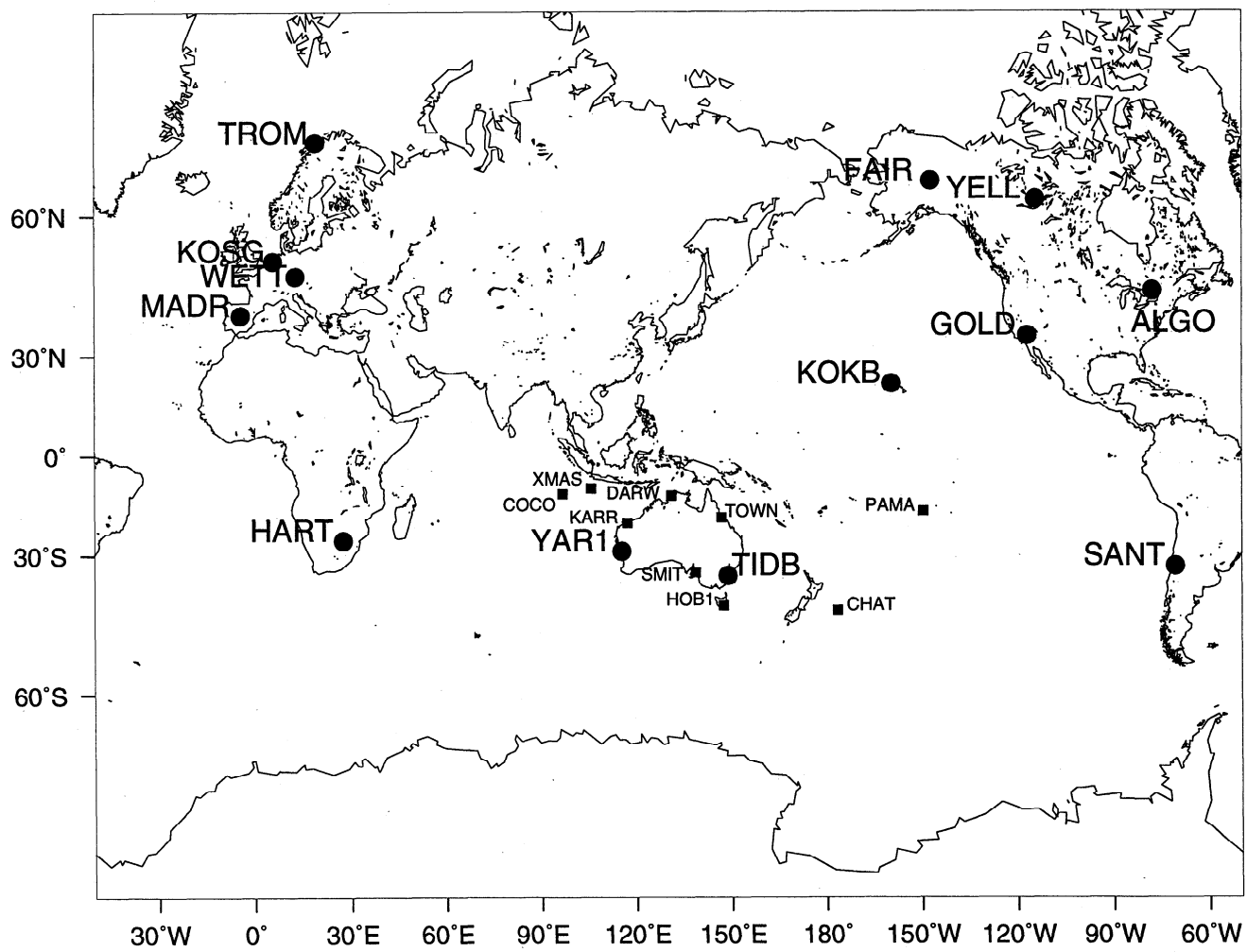

Figure 4. The location of core International GPS Service for Geodynamics sites (circles) and sites beyond the PNG region (small squares) which were used in the computation of the Euler poles of the Australian and Pacific Plates.

Of the separate annual solutions those for the 1990 campaign are the least precise because of the smaller available satellite constellation in 1990, the sparse global tracking network which was operating at that time, and the quality of the GPS receivers used. Thus the velocity estimate of WITU, which was observed only in 1990 and 1996, has a larger uncertainty than that of the other sites (Table 1 and Figure 6). Where two different marks were occupied (Guasopa and

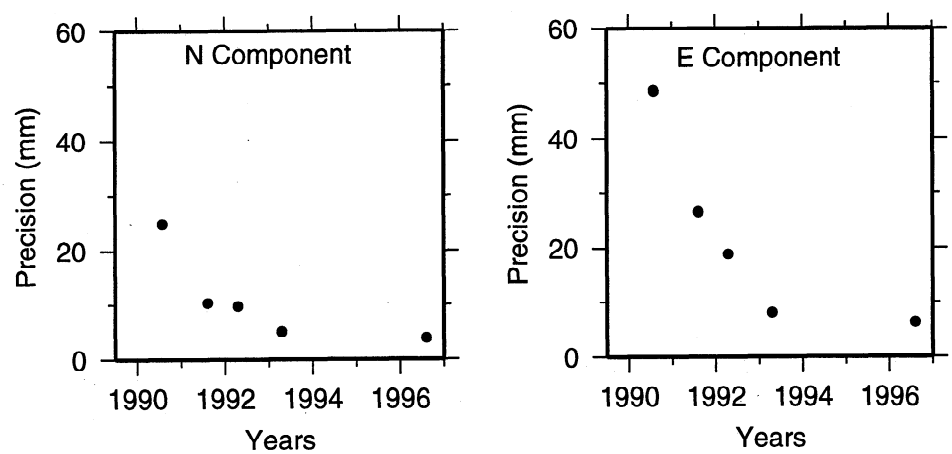

Figure 5. The precision of local north and east coordinate estimates of each campaign from daily repeatability studies.

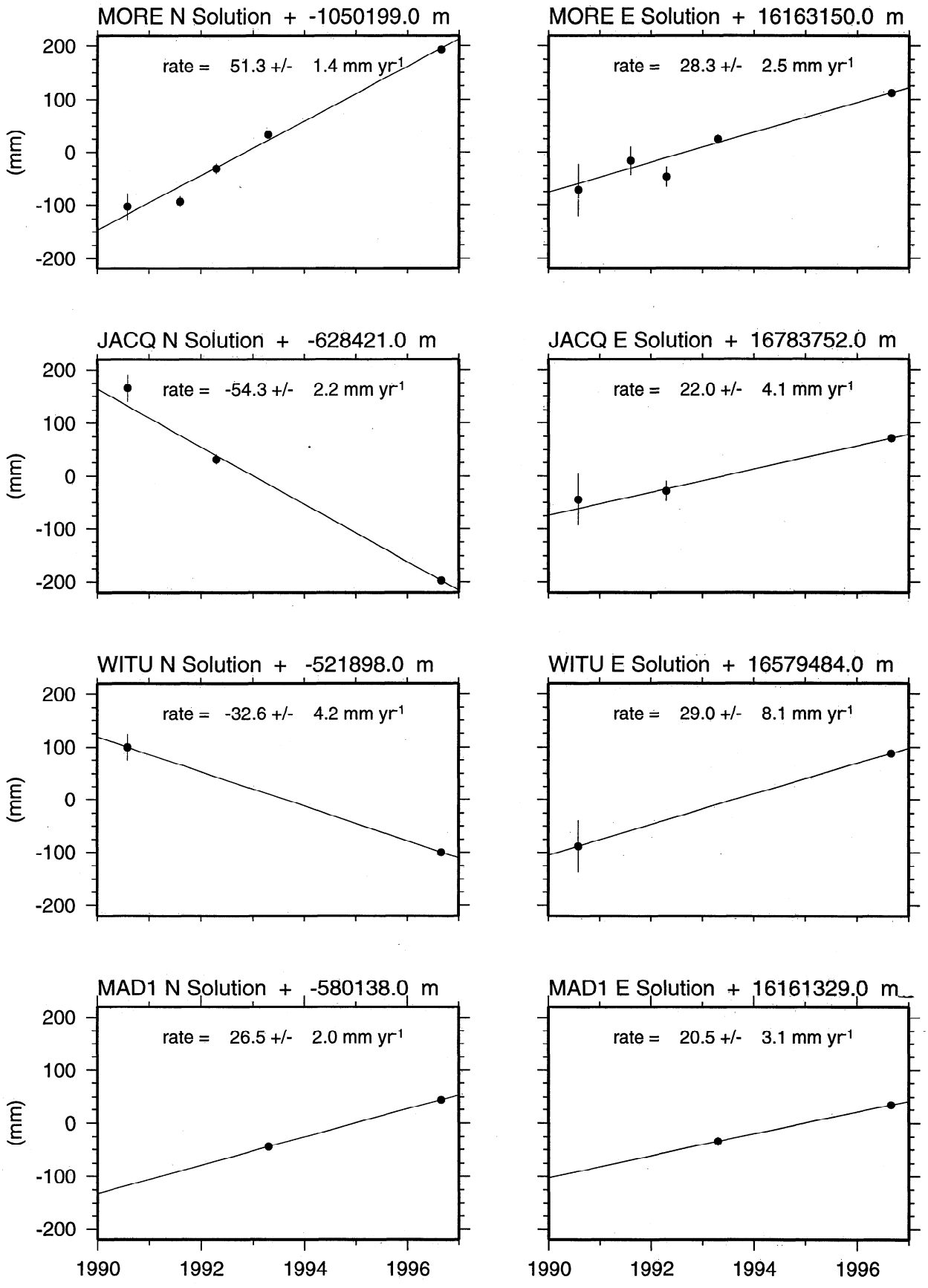

Figure 6. The velocity estimates in local coordinate system, and errors associated with the slope of the linear regression line for some sites in the PNG network.

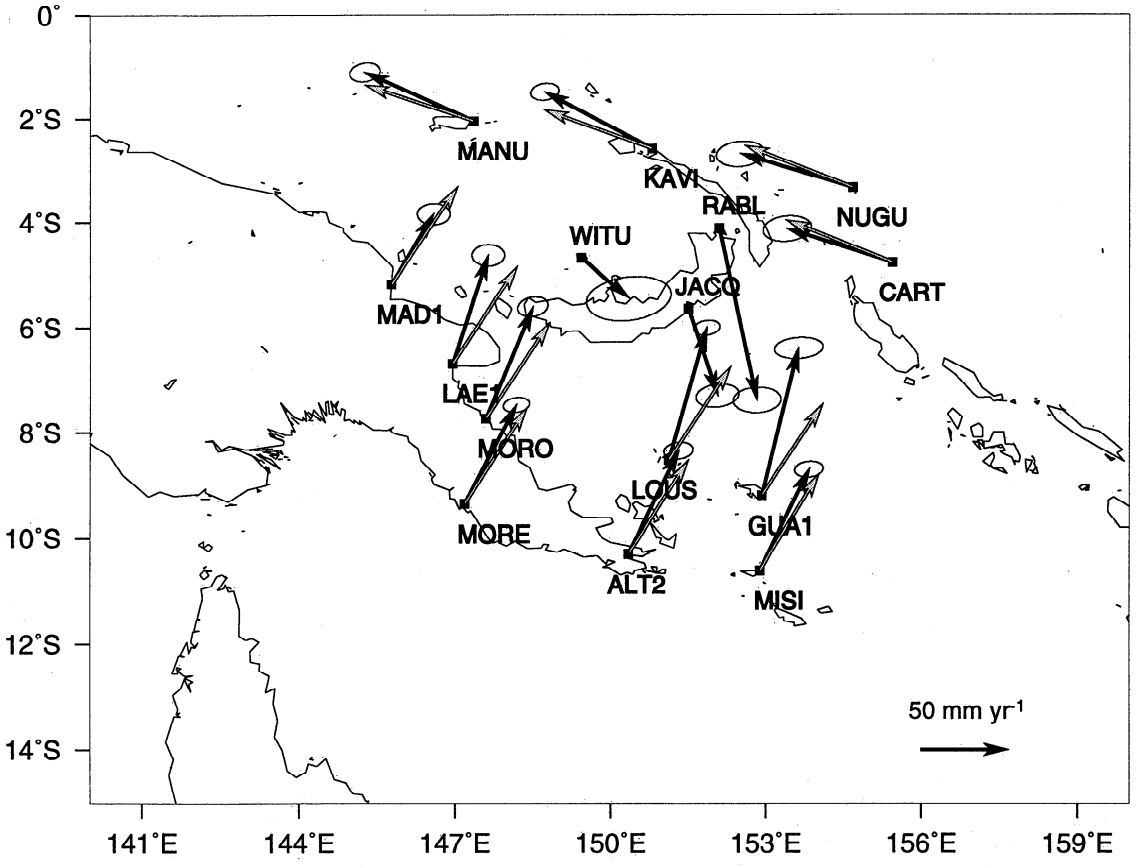

Figure 7. The absolute GPS velocities (solid arrows) and corresponding 99% error ellipses. NNR1A velocities (open arrows) are shown for MAD1, LAE1, MORO, MORE, ALT2, MISI, LOUS, and GUA1 (Australian Plate) and for MANU, KAVI, NUGU, and CART (Pacific Plate).

Misima), the estimated velocities for each mark are in good agreement and lie well within the uncertainties of the individual determinations (Table 1).

4.2. Site Motions

To test whether our estimated velocities agree with the NNR1A plate model velocities, we compared our vectors and uncertainties with the motion of a site when modeled by the Euler pole for a particular plate in the NNR1A model (which does not provide information of the uncertainties of the estimates). We consider that if the NNR1A estimate lies within 2σ (or the 95% confidence limit) of our velocity estimate, then statistically the two vectors are not significantly different, indicating that our estimated velocity can be considered to represent motion of that particular plate in the NNR1A model. Similarly, if an estimated rate of change in baseline length between two sites is not significantly different from zero, we conclude that the baseline length has remained "constant" or unchanged for the duration of the observations.

Figure 7 illustrates the geodetic estimates for the ITRF94 absolute site velocities and the geological predicted motions from the NNR1A plate model. When considering the previously mentioned discrepancies of 1-2 mm yr^{-1} between the two reference frames and the unpublished uncertainties of the NNR1A model, we conclude that the velocities of MISI, ALT2, and MORE are consistent with the motion of the Australian Plate, and NUGU, CART, MANU, and KAVI are consistent with the motion of the Pacific Plate to within ~5-9 mm yr^{-1} (the 99% confidence level). This is examined further in Table 3 where the changes in the baseline lengths within these two groups of sites are clearly not significantly different from zero, consistent with these sites being located on the same plate. The observed velocities of the remaining sites differ from the predictions based on the NNR1A model, indicating that they do not lie on either of the two major plates. Baseline lengths between some of these sites exhibit significant variations with time, suggesting the existence of small tectonic units between the Australian and Pacific Plates.

The velocities of the two sites in the Solomon Sea, LOUS, and GUA1, show significant differences from the motion of the Australian Plate, while the baseline length between GUA1 and LOUS remains constant at the 95% confidence level (Table 3). This is consistent with the occurrence of spreading on the Woodlark Basin Spreading Centre. The estimated full rate of spreading between GUA1 and MISI is 26.4 ± 5.0 mm yr^{-1} while that between LOUS and ALT2 is 12.6 ± 4.6 mm yr^{-1}, suggesting that the relative pole lies to the west of the Papuan Peninsula. No significant relative motion is evident between GUA1, LOUS, MORO, and LAE1, suggesting that the four sites may lie on the same plate, the Woodlark Plate. The MORO and LAE1 velocities are significantly different to the Australian Plate velocities, and there is no significant motion between these two sites at the 95% confidence level. The baselines

Table 3. Changes in Baseline Lengths (mm yr^{-1}) and Associated 95% Confidence Intervals

	JACQ	MAD1	WITU			
JACQ	-					
MAD1	-0.4±8.0	-				
WITU	1.3±13.6	-5.3±13.2	-			
	CART	KAVI	MANU	NUGU		
CART	-					
KAVI	6.4±8.4	-				
MANU	4.2±8.6	-0.1±6.0	-			
NUGU	1.9±8.0	-0.5±8.6	-0.9±8.6	-		
	ALT2	MISI	MORE	MORO	LAE1	LOUS
ALT2	-					
MISI	-0.4±7.8	-				
MORE	-0.5±7.0	-0.7±6.2	-			
MORO	5.3±6.6	4.9±6.4	6.2±4.6	-		
LAE1	8.6±6.6	9.8±6.4	6.0±5.0	1.8±5.8	-	
LOUS	12.6±4.6	18.4±5.2	-2.4±5.2	-6.8±6.0	-3.5±6.0	-
GUA1	2.7±8.6	26.4±5.0	-6.5±8.0	-10.3±8.2	-7.3±8.2	-3.7±7.8

MORE-LAE1 and MORE-MORO both show a small but significant rate of divergence at the 95% confidence level but not at the 99% level.

The velocity estimates of RABL and JACQ differ by 50 mm yr^{-1}. Both sites are in New Britain, and this difference is too large to be explained with rigid plate theory. On September 19, 1994, two volcanic eruptions occurred in the Rabaul caldera (Tavurvur and Vulcan) ~7 km from the RABL site [*McKee et al.*, 1995]. The RABL GPS mark is located at the Rabaul Volcanological Observatory (RVO), which is actually within the caldera. The eruptions occurred between the two occupations of RABL (1992 and 1996), and we considered that the estimate of the velocity of RABL contained a component of local deformation due to the eruptions and excluded this site from further tectonic interpretations. Future reoccupations of RABL should provide further insight into this anomalous result.

The velocities of MAD1, JACQ and WITU are significantly different from either the Australian or Pacific Plate velocities (i.e., residual velocities >20 mm yr^{-1}). The baseline lengths between the three sites remain constant with time, consistent with these sites being located on a small plate which is rotating in a clockwise direction.

KAVI has been occupied during four different campaigns,

Table 4. Absolute Euler Pole Estimates

Plate	Latitude (°)	Longitude (°)	Rate (° Myr^{-1})	Pole Error Ellipse		
				σ_{max} (°)	σ_{min} (°)	Azimuth (°)
Australia[a]	31.6	41.3	0.62 ± 0.01	2.89	1.36	293
Pacific[b]	-61.4	105.0	0.63 ± 01	2.80	1.13	54
Woodlark[c]	-0.7	128.4	1.78 ± 0.30	4.20	0.65	289
South Bismarck[d]	6.7	-31.7	8.15 ± 0.30	0.22	0.15	358

Rotation is in an anti clockwise direction about the pole. The error ellipses of poles are described by the one sigma semi-major and semi-minor axes of each error ellipse and the clockwise angle from north of the semi-major axis.

[a] Pole position based on the velocities of KARR, YAR1, COCO, XMAS, SMIT, TIDB, TOWN, HOB1, and DARW.

[b] Pole position based on the velocities of KOKB, PAMA, CART, NUGU, KAVI, MANU, and CHAT.

[c] Pole position based on the velocities of LOUS, GUA1, LAE1, and MORO.

[d] Pole position based on the velocities of JACQ, WITU, and MAD1.

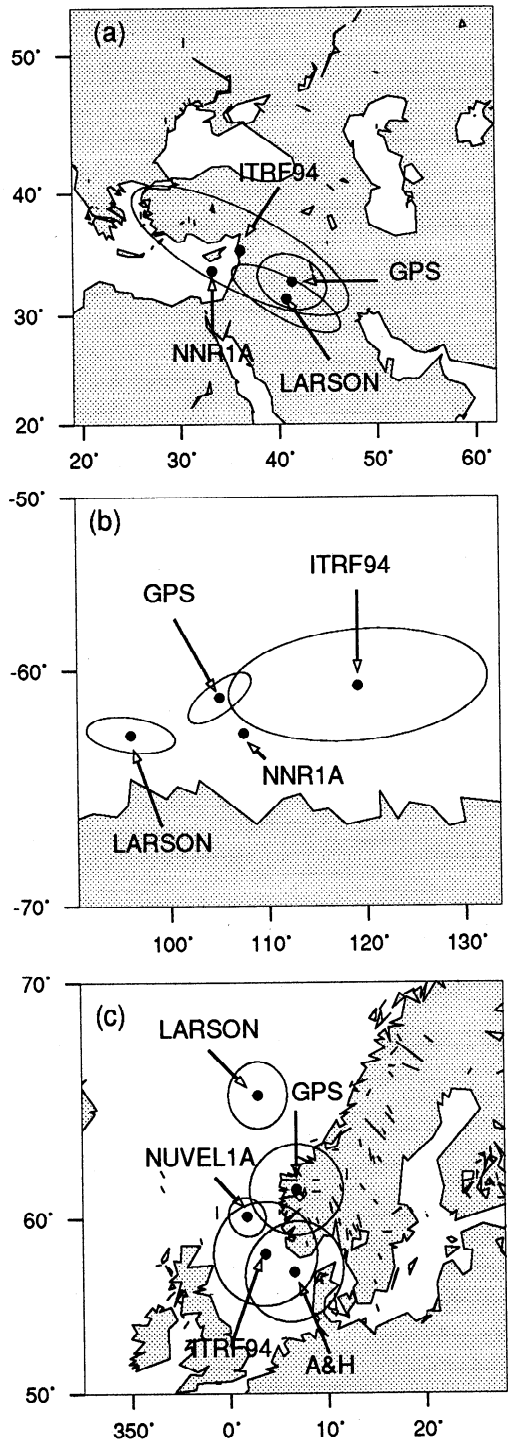

Figure 8. The location of Euler poles: (a) Australian Plate, (b) Pacific Plate, and (c) Australian-Pacific relative pole. Our GPS estimate, NNR1A, NUVEL-1A [*DeMets et al.*, 1994] (Figure 8c), and ITRF94 as well as the poles determined by *Larson et al.* [1998] (LARSON) and *Argus and Heflin* [1995] (A&H) are plotted. The 95% error ellipses are shown where available.

and its velocity is well determined. It does show some northerly motion relative to the Pacific Plate (Figure 9 below). However, the discrepancy lies within the 99% error ellipse of the velocity, and changes in the baseline lengths between this site and NUGU, CART, and MANU are not significantly different from zero. The MANU velocity also shows some northward motion relative to the Pacific Plate, although this falls within the 95% error ellipse. It is possible that this spatially concurrent motion is indicative of a block movement northward relative to the Pacific Plate, but our resolution is not sufficiently precise for us to make a definitive statement. We conclude that to within our measurement uncertainties, KAVI lies on the Pacific Plate.

Mobbs [1997] concluded that MANU and KAVI were located on the Pacific Plate and that MORE, ALT2, MISI, MORO, GUA1, UNIT, and LOUS were located on the Australian Plate to within the uncertainty of the measurements (1σ level of ~±15 mm yr^{-1}). By analyzing additional GPS data we have improved the accuracy of the velocity estimates which has led to a more detailed velocity field for the PNG region and has shown that MAD1, MORO, LAE1, LOUS, and GUA1 are not moving with the Australian Plate.

4.3. Euler Pole Estimates

Using our velocity estimates for the PNG sites as well as other IGS sites, we computed Euler poles for the Australian, Pacific, Woodlark, and South Bismarck Plates (Table 4), with only the first two of these plates being contained in the NNR1A model. Figure 8 compares these poles with the NNR1A estimates. Differences are minor and change the velocity predictions at the sites by less than the uncertainties of the velocities (for example, differences of 2.8 mm yr^{-1} north and 0.4 mm yr^{-1} east for YAR1, 2.1 mm yr^{-1} north and 1.5 mm yr^{-1} east for TIDB). We compute the relative convergence between the Australian and Pacific Plates in the PNG region to be 98 mm yr^{-1} at a bearing of 18° which is slightly slower than the NUVEL1-A estimate of 103 mm yr^{-1} at a bearing of 17° [*DeMets et al.*, 1994]. *Larson et al.* [1998] also computed Euler poles for the Australian and Pacific Plates using GPS-derived velocities from sites with more than 2 years of continuous observations. Their estimate of the position of the Australian pole agrees with our estimate, but the location of their Pacific pole is quite different in longitude (see Figure 8b). Since we used more sites giving a wider geometrical distribution across the Pacific Plate, our determination of the Pacific Plate Euler pole is more reliable.

Geodetic determinations of the poles of these two plates from GPS [*Argus and Heflin*, 1995] and from the velocities of sites in ITRF94 are also illustrated in Figure 8. The 95% confidence interval error ellipse of our Australian-Pacific relative pole overlaps the error ellipses of the NUVEL-1A [*DeMets et al.*, 1994], the ITRF94, and the *Argus and Heflin* [1995] determined relative poles for these two plates. However, the solution is significantly different to the relative pole of *Larson et al.* [1998] (Figure 8c).

The velocities of LOUS, GUA1, MORO, and LAE1 can be modeled to within their uncertainty by a rotation about a single Euler pole (Figure 9). Similarly, the motions of MAD1, JACQ, and WITU can be modeled by a clockwise rotation about a pole located in the Huon Gulf. Since the geometrical locations of these three sites are well separated in azimuth relative to the pole of rotation, the pole for the South Bismarck Plate is more precisely determined (by a factor of 2) than all the other poles we have estimated, hence the relative error ellipses of the South Bismarck Plate with respect to all other plates are small, ~4 times smaller than the relative error ellipses for the models of *Argus and Heflin* [1995] and NUVEL1 [*DeMets et al.*, 1990]. The size of the error ellipse Australian/Woodlark relative pole is consistent with the

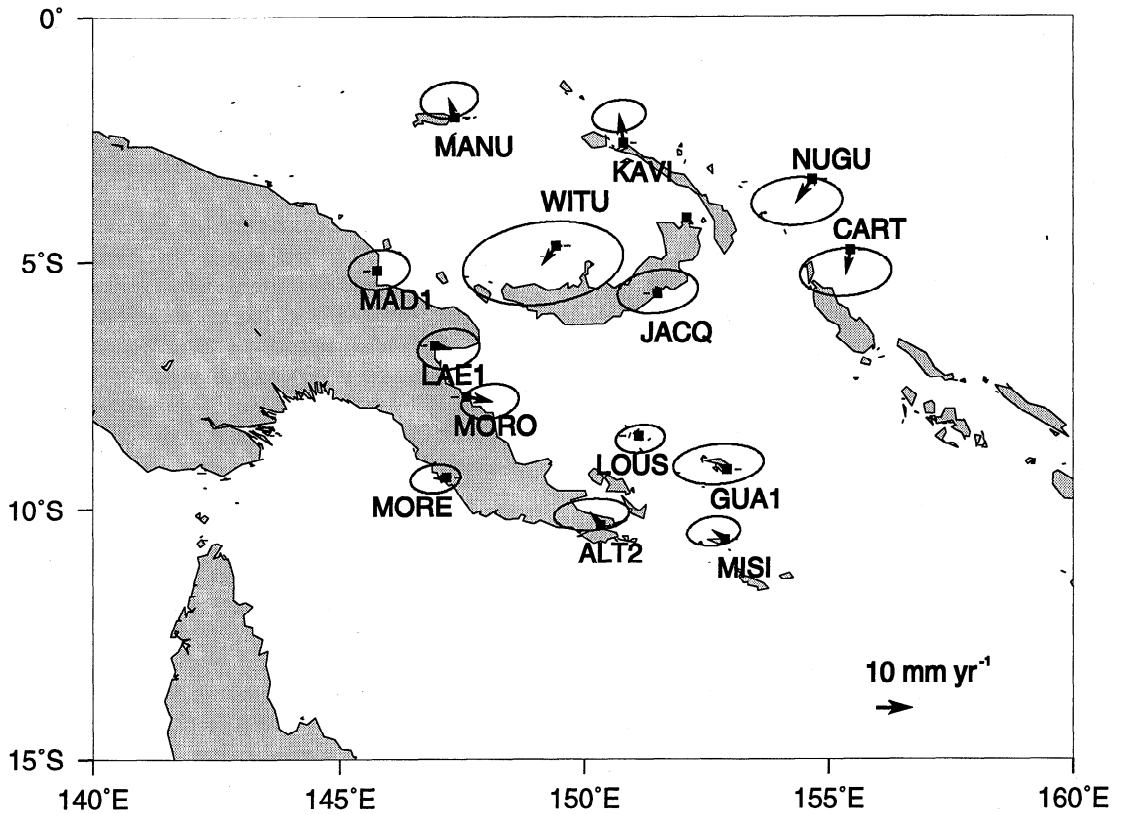

Figure 9. The residual GPS vectors with respect to our predicted motions using Euler poles in Table 5.

uncertainties of relative poles of other investigators. This is due to the geometry of the geographical locations of sites on the Woodlark Plate rather than to inferior estimates of the site velocities.

4.4. New Plate Model

We propose a five-plate model to represent the present-day kinematics of the PNG region (Figure 10): Australian, Pacific, Solomon Sea, Woodlark, and South Bismarck Plates (although we cannot distinguish between the Solomon Sea and Woodlark Plates with our data). The three minor plates accommodate the convergence of the two major plates, the Australian and Pacific Plates. The Australian Plate extends as far north as the southern part of the Papuan Peninsula (including the Port Moresby, Alotau, and Misima sites), while the islands of Nuguria, Carteret, Manus, and northern New Ireland are on the Pacific Plate. Madang, Witu, and Jacquinot Bay are located on the South Bismarck Plate and Lae, Morobe, Losuia, and Woodlark Island are located on the Woodlark Plate. Our GPS-observed velocities fit this five-plate model at a 95% confidence level (or <8 mm yr^{-1}) with the exception of KAVI (as discussed above).

5. Discussion

In the recent past the Solomon Sea Plate has subducted beneath the Australian and South Bismarck Plates at the Trobriand Trough and the New Britain Trench. Subduction is still occurring on the New Britain Trench, but activity has virtually ceased on the Trobriand Trough with recent geological convergence estimates ranging from ~6 [*Kirchoff-Stein*, 1992] to 20 mm yr^{-1} [*Eiichi et al.*, 1986]. The oceanic lithosphere south of the Trobriand Trough has an absolute velocity of ~80 mm yr^{-1} with an azimuth of ~14° (at 153°E), so we infer that the Solomon Sea Plate is now moving at a similar rate.

The Australian/South Bismarck continent-arc collision occurred at ~3-4 Ma, while the Woodlark Basin Spreading Centre has been active for about the last 4 Myr [*Benes et al.*, 1994]. The block north of the Woodlark Basin Spreading Centre (which we have referred to as the Woodlark Plate) was once a part of the Australian Plate but is now in the process of separating from it. Continental rifting is propagating northwestward into the Papuan Peninsula with a small rate of divergence occurring across the Owen Stanley Range. There is no definite boundary between the Woodlark and Australian Plates on the Papuan Peninsula further northwest of ~148°E because in this region the two plates have not yet begun to separate.

Below we compare our model derived from geodetic data to the geological and seismic data of the region and show that it is consistent with all three types of data. We use our Euler poles to determine current motions at the plate boundaries and to compare these to estimates obtained from geology and seismicity.

5.1. Definition of Plates

5.1.1. South Bismarck Plate. We define the South Bismarck Plate to be bounded by the Bismarck Sea Seismic Lineation in the north and the New Britain Trench in the south. The eastern boundary is ill defined, although there are a number of left-lateral faults in the region which may be the

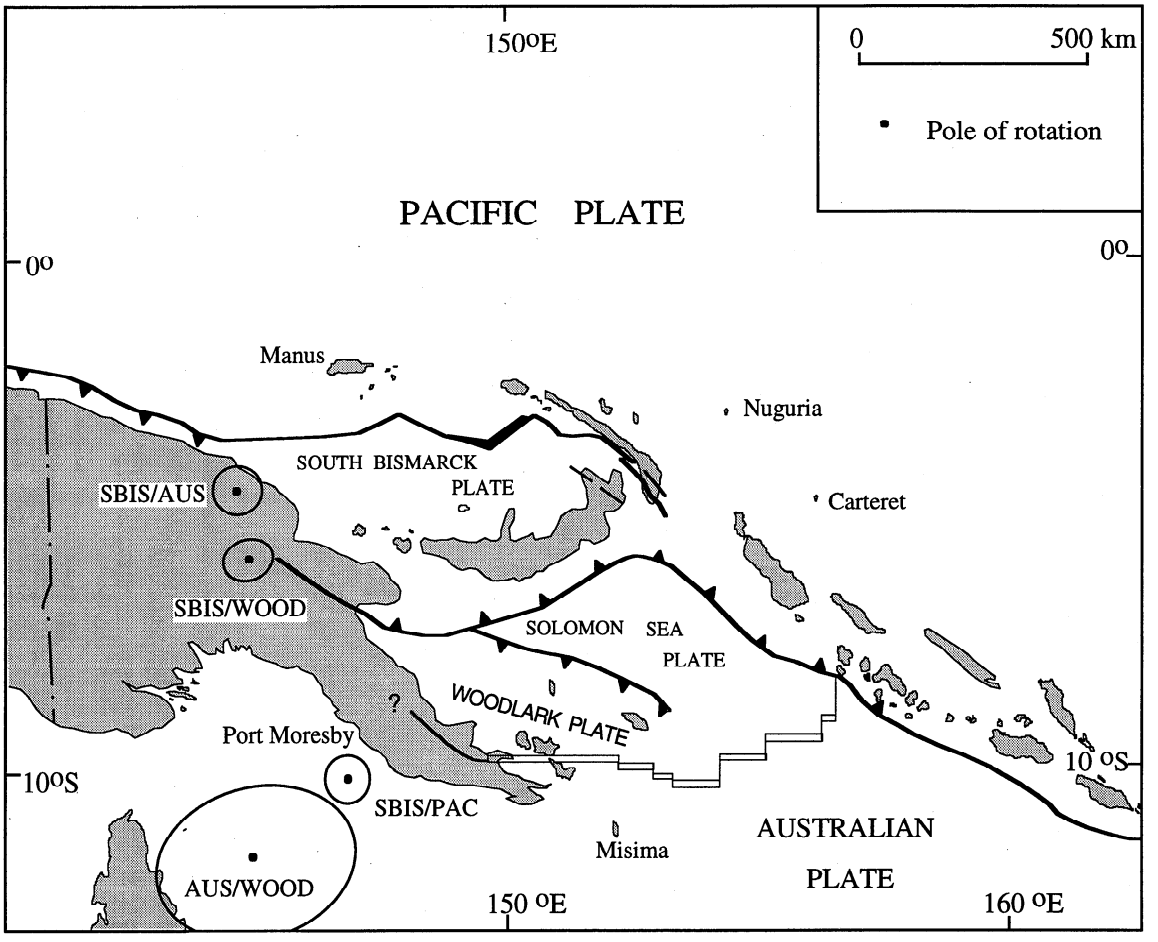

Figure 10. The proposed tectonic boundaries and relative Euler poles based mainly on the GPS data. The error ellipses plotted on the Euler poles represent the 95% confidence level.

continuation of the lineation. Clearly, though, the boundary is west of the islands of Nuguria and Carteret. The western boundary is a continent-island arc collision occurring on the Ramu-Markham Fault and beneath the Finisterre Range. The plate extends at least as far westward as Madang, but without further geodetic measurements we cannot define the western end of the South Bismarck Plate. We presume that this is somewhere near Wewak, where the Wewak Trench begins. Geologically, the western limit of the continent-arc collision would be the Adelbert Range northwest of Madang.

5.1.2. Solomon Sea/Woodlark Plates. As already mentioned above, we distinguish between the Solomon Sea and the Woodlark Plates only on the basis of the seismic and geological evidence [e.g., *Pegler et al.*, 1995; *Cooper and Taylor*, 1987a]. If the Solomon Sea Plate exists in the form of a doubly dipping slab beneath the Finisterre Range and Papuan Peninsula as shown by *Pegler et al.* [1995], then clearly the Trobriand Trough has been an active subduction zone in the past. Hence, in the past the Solomon Sea Plate and the lithosphere to the south of the Trobriand Trough belonged to different plates. We distinguish between the Solomon Sea Plate and Woodlark Plates on the basis that there was relative motion in the recent past and choose to retain the Trobriand Trough as the southwestern boundary of the Solomon Sea Plate. The northern and eastern boundaries are the New Britain and San Cristobal Trenches.

The Woodlark Basin Spreading Centre forms the southern boundary of the Woodlark Plate. The boundary becomes a continental rift zone with divergence across the Papuan Peninsula as far west as 148°E. It then becomes a left-lateral shear zone with a small compressional component increasing westward. The deformation in this area is probably diffuse and widely distributed.

5.1.3. Is there a North Bismarck Plate?. We find no conclusive evidence for a North Bismarck Plate at the 99% confidence level, although the spatial conformity of the residual motion of MANU and KAVI relative to the Pacific Plate suggests that there may be some differential motion between these sites and the Pacific Plate but of a magnitude (<8 mm yr^{-1}) that is below our current resolution. This would be consistent with the existence of a North Bismarck Plate with slow convergence occurring at the Manus Trench. Alternatively, the residual motion at KAVI (significant at the 95% confidence level) might be a localized effect associated with the very active spreading segment of the Bismarck Sea Seismic Lineation located southwest of the northern tip of New Ireland.

5.2. Motion at Plate Boundaries

5.2.1. Solomon Sea-South Bismarck Plates. We cannot unequivocally solve for relative motion at the New Britain Trench because our GPS measurements cross both the

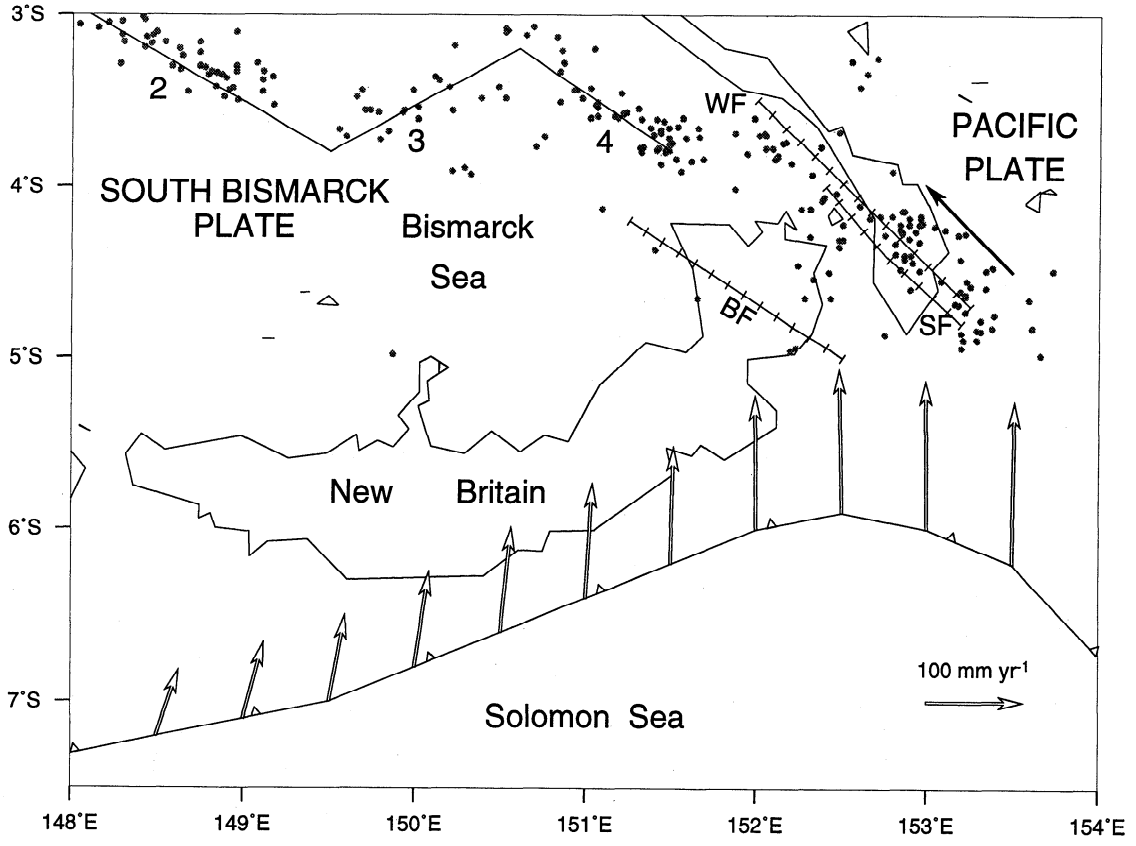

Figure 11. The predicted motion of the Solomon Sea Plate relative to the South Bismarck Plate at the New Britain Trench (open arrows) and motion of the Pacific Plate relative to the South Bismarck Plate in southern New Ireland (solid arrow). Shallow earthquakes (0-50 km) shown north of 5°S indicate the most likely boundary between the South Bismarck and Pacific Plates. Earthquakes south of 5°S are dominated by subduction-related events and are omitted. Numbered segments of the Bismarck Sea Sesimic Lineation are indicated [*Taylor*, 1979]. BF is the Baining Fault; SF is the Sapom Fault; and WF is the Weitin Fault.

Trobriand Trough and the New Britain Trench. If we assume that the pole for the Woodlark Plate also represents the motion of the Solomon Sea Plate, the computed rate of subduction on the New Britain Trench varies from 80 mm yr^{-1} in the west to 150 mm yr^{-1} in the east (Figure 11). The motion is slightly oblique, at an angle of 20° to the trench at the western end, but becomes normal eastward along the trench. It becomes very oblique at the eastern end where the trench turns sharply southward, but the overriding plate in this region is not the South Bismarck Plate, and hence our relative Euler pole will not be valid here.

Abers and McCaffrey [1994] computed a set of slip vectors from earthquakes in the PNG region and showed that the azimuths of these vectors on the New Britain Trench do not vary smoothly, rather they show a discontinuity at 149°E where they change suddenly from ~20° to 0°. They claimed that an additional 50 mm yr^{-1} of right-lateral shear is required in order to accommodate this slip vector discrepancy and that the motion of the plates cannot be represented by a single relative pole. *Pegler et al.* [1995] noted that this is a consequence of two different plates being involved in the collision with the South Bismarck Plate. Our prediction disagrees with the slip vector azimuths of *Abers and McCaffrey* [1994] as far east as 151°E, at which point our predicted convergence also becomes normal to the trench. This difference may result from localized deformation within the subducted slab, or it may be that slow subduction at the Trobriand Trough renders our Woodlark/South Bismarck relative pole inappropriate for predicting motion at the western end of the Solomon Sea/South Bismarck plate boundary.

5.2.2. South Bismarck-Pacific Plates. The boundary between the South Bismarck and Pacific Plates probably stretches from the Wewak Trench in the west to the triple junction with the New Britain Trench in the east. This boundary is a transform fault along the western sections of the Bismarck Sea Seismic Lineation which then becomes a very fast spreading center just west of New Ireland, and finally turns into a left-lateral strike slip zone through southern New Ireland. The expected relative motion in southern New Ireland (4.5°S, 153°E) is 130 mm yr^{-1} at a bearing of 316° (Figure 11), parallel to the many strike slip faults in this region which may accommodate this motion. Figure 11 shows the shallow earthquakes (0-50 km) which have occurred in this region between 1964 and 1994 and the faults which have been identified in the region. These distributions suggest that the motion at this boundary must be partitioned across a number of left-lateral faults.

The expected spreading on the third segment of the Bismarck Sea Seismic Lineation is 141 mm yr^{-1} in a direction

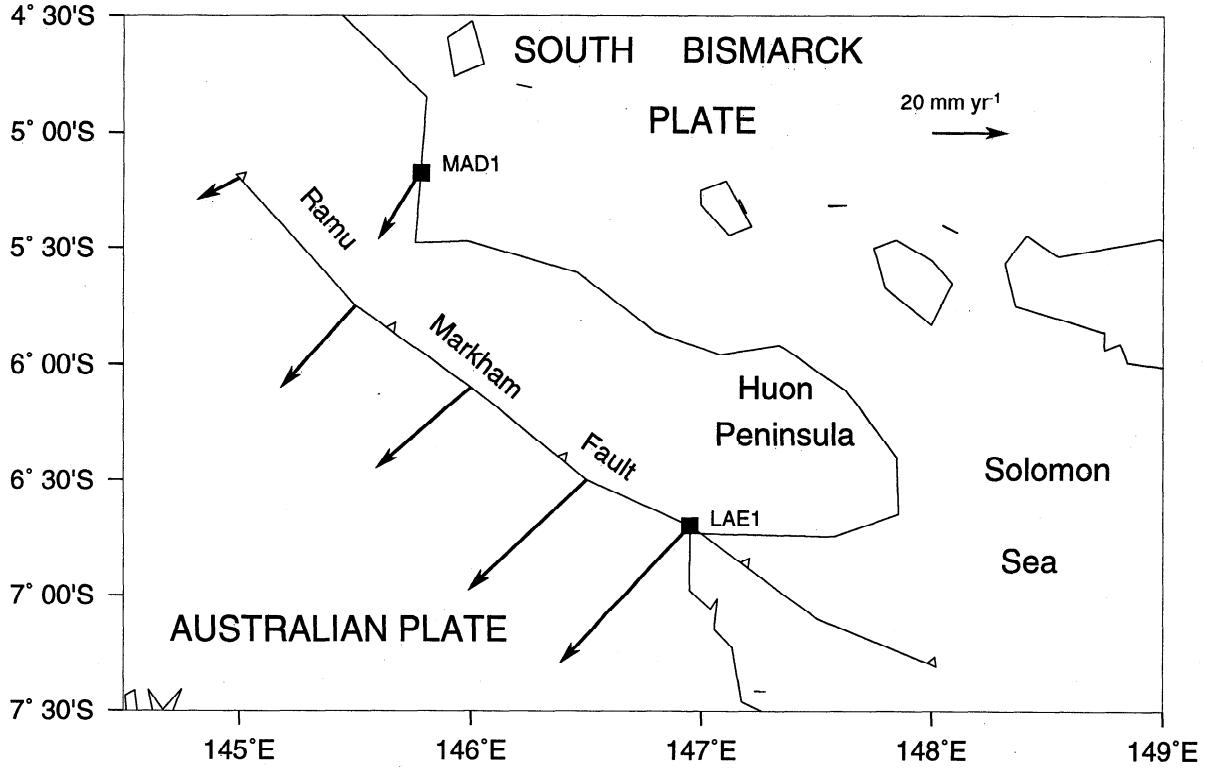

Figure 12. The predicted motion of the South Bismarck Plate relative to the Australian Plate at the Ramu-Markham Valley Fault.

of 297° (orthogonal to the spreading axis) which is the fastest relative motion across any boundary in the whole PNG region. Our estimate of this motion is in agreement with *Taylor* [1979], who estimated the spreading to be ~130 mm yr^{-1} on the basis of the magnetic anomaly data.

5.2.3. South Bismarck-Australian Plates. The collision between the Australian and South Bismarck Plates is accommodated in the Finisterre Range, the New Guinea Highlands, and the Markham Valley, although the boundary between the plates is probably the Ramu-Markham Fault. Assuming that the total collision is taken up on this fault, the predicted pattern of convergence is essentially frontal becoming more oblique toward the west but with a significant reduction in magnitude (Figure 12). Because the relative pole of rotation of the Australian/South Bismarck Plates (Table 5) is very close to the collision zone, any small change in position of either the pole or the assumed collision zone will cause significant changes in the azimuths of the relative motion across the boundary, whilst the magnitude will remain unchanged. We conclude that there is ~29 mm yr^{-1} of convergence occurring between the two plates at 145°30'E, increasing to 50 mm yr^{-1} at 147°E. This is consistent with the

Table 5. Relative Euler pole estimates

Plates	Latitude (°)	Longitude (°)	Rate (° Myr^{-1})	Pole Error Ellipse σ_{max} (°)	σ_{min} (°)	Azimuth (°)
Australia-Woodlark	-10.8	145.2	1.86±0.03	2.01	1.58	74
South Bismarck-Australia	-4.5	144.6	7.98±0.02	0.49	0.48	5
South Bismarck-Woodlark	-5.7	144.8	9.83±0.02	0.51	0.40	61
South Bismark-Pacific	-10.2	146.9	8.46±0.02	0.45	0.45	1
Pacific-Australia	61.4	6.8	1.01±0.02	2.38	2.28	84

Rotation of the second plate relative to the first plate is in an anti clockwise direction about the pole. The error ellipses of the poles are described by the one sigma semi-major and semi-minor axes of each error ellipse and the clockwise angle from north of the semi-major axis.

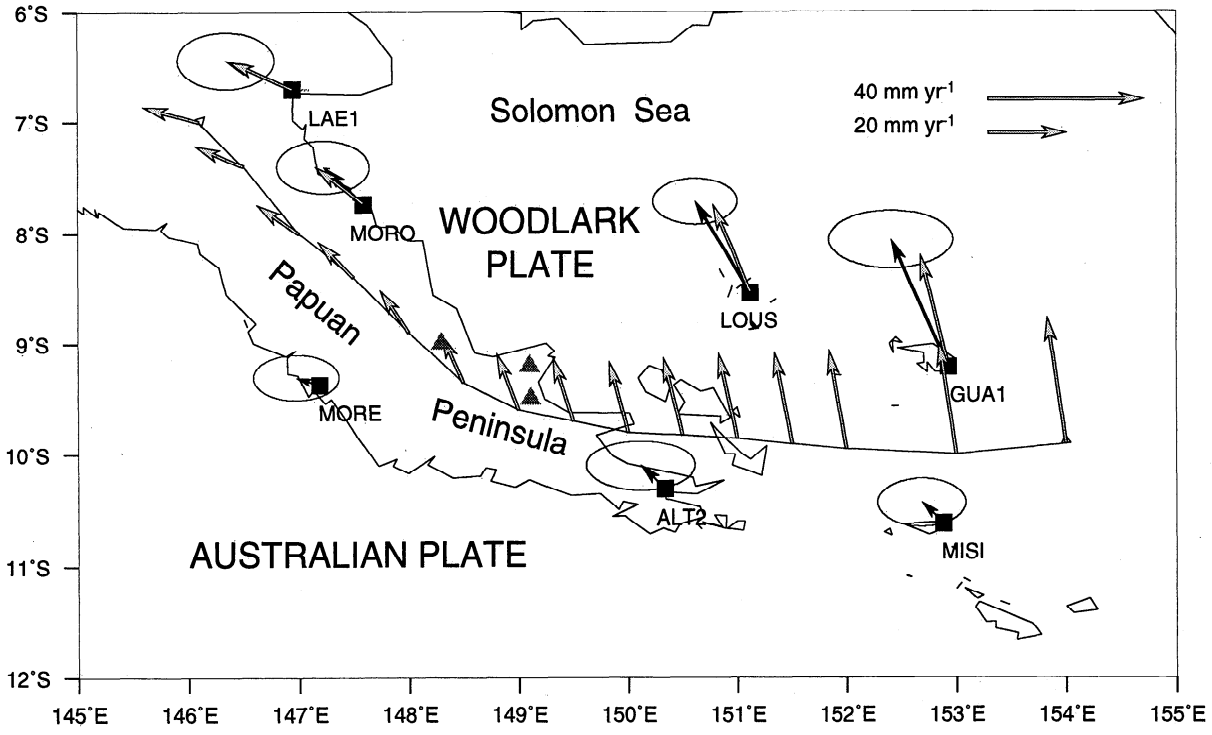

Figure 13. The predicted motion of the Woodlark Plate with respect to the Australian Plate at the Woodlark Basin Spreading Centre and the Papuan Peninsula. The solid arrows represent the residual GPS vector relative to the Australian Plate. The open arrows represent the predicted relative motion using our estimate of the Australian/Woodlark relative Euler pole. The 95% error ellipses are plotted. The active volcanoes on the Papuan Peninsula are indicated with triangles.

geological evidence for the Finisterre terrain being amalgamated with the Australian Plate from the northwest to the southeast in the last 3 Myr [*Abbott et al.*, 1994].

5.2.4. Woodlark-Australian Plates. Spreading is well defined on the Woodlark Basin Spreading Centre, and our model predicts a half-spreading rate of 12 mm yr^{-1} at 153°E, increasing to 40 mm yr^{-1} at 156°E (Figure 13). This is about half the rate determined from magnetic reversals by *Benes et al.* [1994]. Their relative pole position (9°30'S, 148°56'E) is located to the east of our estimate (Table 5), but they do not provide any estimate of uncertainty of their pole position or rotation rate. If there is a significant difference between the rate estimates from a history of magnetic reversals and from recent GPS measurements, then this indicates that the rate of spreading is slowing down or has slowed in recent times. This would be a significant finding since in most cases there has been very good agreement between estimates of motion from geological and geodetic information [see, e.g., *Robbins et al.*, 1993; *Argus and Heflin*, 1995; *Larson et al.*, 1998].

A slowing down of spreading on the Woodlark Basin Spreading Centre might indicate that the spreading was a temporary response to structural tensions rather than long-lived forces in the lithosphere. *Goodliffe et al.* [1997] showed from sidescan and multibeam bathymetry surveys that the whole spreading center reoriented synchronously at ~80 ka and suggested that such a reorientation could be caused by a large and rapid change in local plate motions. If a reorientation occurred, the spreading rates before and after such an event will not necessarily be the same, and owing to the lack of magnetic reversals in the past 200 kyr, it is not possible to determine a change in spreading rate from magnetic anomalies. *Goodliffe et al.* [1997] estimated that the reorientation occurred at ~80 ka, assuming that the estimate of the rate of spreading from magnetic anomalies was valid both before and after the reorientation. Assuming that the spreading rate estimated from the magnetic anomaly data represents the motion prior to reorientation and that our estimated rate of spreading in the past 6 years represents the motion after the reorientation, we estimate that the reorientation occurred at ~170 ka.

The Woodlark Basin Spreading Centre terminates in the west at the Papuan Peninsula but continues northwestward as a continental rift with recent volcanism in this region being clearly related to continental rifting [*Benes et al.*, 1994]. Our model predicts that the extensional forces in the peninsula will change to strike-slip at ~148°E, which coincides with the area where the volcanism ceases. Further to the northwest, the forces become compressional. We cannot unequivocally determine from our geodetic results where the western end of the Woodlark Plate is located, but the boundary must lie between Port Moresby and Morobe. Our model suggests that there is ~10 mm yr^{-1} of left-lateral slip occurring in the Owen Stanley Range, which gradually becomes orthogonal divergence across the Woodlark Basin Spreading Centre further to the east. Active left-lateral strike-slip faults have been mapped striking NW-SE on the Papuan Peninsula [*Davies et al.*, 1984] which could accommodate this motion. Further

observations on a more dense geodetic network are required across the Papuan Peninsula in order to detect and model the deformation pattern.

6. Conclusions

We have estimated site velocities with respect to ITRF94 using GPS observations spanning 1990-1996. We conclude that there are three microplates trapped in the convergence between the Australian and Pacific Plates. We have estimated poles of rotation of the Pacific, Australian, South Bismarck, and Woodlark Plates and have studied the relative motions across the plate boundaries using these poles. Subduction is occurring on the New Britain Trench at a rate of ~100-130 mm yr^{-1}, convergence of 20-50 mm yr^{-1} occurs between the Australian and South Bismarck Plates, and the rate of spreading on the Woodlark Basin Spreading Centre is about half of the rate determined by *Benes et al.* [1994] from magnetic reversals.

This research identifies a number of interesting areas where future investigations using GPS can provide new information. What is the localized deformation pattern of the collision of the Australian/South Bismarck Plates? Where and how is the predicted strike-slip motion in the Papuan Peninsula accommodated? Did local deformation occur at Rabaul as a result of the 1994 volcanic eruptions? How is the 130 mm yr^{-1} of relative strike-slip motion between the South Bismarck and Pacific plates accommodated? Is there relative motion occurring between northern New Ireland and the Pacific Plate or is this a local effect resulting from the close proximity to the Bismarck Sea Seismic Lineation? Will the eastern tip of the Huon Peninsula show very small absolute motion as a result of being located ~60 km from the pole of the South Bismarck Plate? Is the spreading on the Woodlark Basin Spreading Centre slowing down, or did it slow to a different but constant rate when the spreading center reoriented at ~170 ka? Future GPS campaigns will address these and other issues raised in this paper.

Appendix A: GPS Data Analysis

We describe below some pertinent issues of the analysis of the GPS phase observations using the GAMIT/GLOBK software. Further explanations can be found in, for example *Herring et al.* [1990], *Feigl et al.* [1993], *King and Bock* [1996], and T.A. Herring (1997).

Carrier phase measurements were used in the GAMIT software to estimate 15 orbital parameters per satellite (using the parameter force model of *Beutler et al.* [1994]), three site coordinates and thirteen residual tropospheric delays per station, phase ambiguities (we did not resolve the ambiguities to integer values), and Earth orientation parameters. Depending on the amount of available global tracking data, the data were processed either in a single-network solution per day (1990-1993) or separately as global and regional networks (1996).

The output from a GAMIT solution includes the full variance-covariance matrix of all the parameters and provides the input for the GLOBK Kalman filter in which either multiple GAMIT solutions for a single day, an entire campaign, many years of data, or all of the above are combined. We estimated satellite orbital elements, Earth orientation parameters, and site positions and velocities in GLOBK. Vertical velocities were estimated; however, because of unresolved modeling errors such as antenna phase center variations, we have restricted the discussion in this paper to horizontal velocities. Parameters can be represented in the filter as either linear functions of time or as stochastic variables where variations are modeled as random walk functions with the characteristics of white noise. The correlation between consecutive estimates of a parameter can be controlled: zero noise results in a deterministic estimate of the parameter whereas a large amount of stochastic variation makes each estimate independent of those which precede or follow it [see, e.g., *Herring et al.*, 1990; *Feigl et al.*, 1993; *Tregoning*, 1996; *Hudnut et al.*, 1996]. Stochastic estimation can be used to generate daily estimates of parameters, allowing studies of repeatabilities of site coordinates to be made.

Combining separate GPS solutions with a Kalman filter has important advantages for estimating satellite orbits and for defining the terrestrial reference frame. It has been shown that finite length multiday arcs improve the accuracy of the orbit estimation (and hence station coordinates) by using the orbital dynamics of the satellites as additional information to constrain the orbits [*Beutler et al.*, 1987; *Lichten and Border*, 1987; *Davis et al.*, 1989, *Beutler et al.*, 1996]. We utilized this feature when processing the 1990 to May 1992 solutions by filtering together many daily solutions which refer to the same initial osculating orbital elements, resulting in estimates of the orbit based on many days of data. Because of the small fiducial tracking network operating for this period, we processed all regional and global data simultaneously in daily solutions.

By July 1992 the distribution of sites in the IGS network had significantly improved, and we chose not to estimate multiday arcs for the post July 1992 solutions. We processed global and regional data simultaneously in the 1993 solutions; however, with the current number of IGS global tracking sites it is no longer computationally efficient to process all available data simultaneously, and so we processed the 1996 global and regional data separately and used the filter to estimate a single set of orbital elements from all global and regional solutions of a single day. We used the 1996 daily global analyses computed at the Scripps Orbit and Permanent Array Center, Scripps Institution of Oceanography [*Bock et al.*, 1993].

Another important feature of the Kalman filter relates to the definition of the terrestrial reference frame. The tracking sites which define this system have evolved with time and were not operational in the earlier PNG campaigns for which the global tracking data relied on older (now mostly inoperative) tracking sites. Thus there was a need to project back in time the current knowledge of the definition of the terrestrial reference frame via the coordinates of intermediate tracking sites. This is possible in the computations performed by the Kalman filter using the information contained in the estimates of the parameters and the covariance matrices. We can therefore compute the whole solution relative to ITRF94 even though not all of the input GAMIT solutions contain observations at sites with well-determined ITRF94 coordinates.

We combined all the data spanning 1990-1996, solving for coordinates and velocities of all sites without initially

imposing any reference frame on our solution. We then transformed our loosely constrained network into an externally defined terrestrial reference frame (in this case ITRF94). There are two main advantages of this approach: it is computationally efficient when testing for the effects of different external reference frames on site velocities, and the solution is free of any external constraints or possible distortions until the last step of the procedure.

The data which were filtered in GLOBK included more than just the data of the PNG surveys. We also analysed the Australasian data used by *Tregoning* [1996] in determining the subduction rate across the Java Trench and all available data during the GPS IERS and Geodynamics experiment (GIG'91) [*Blewitt*, 1993]. It was initially thought that this additional data was necessary to maintain a consistent reference frame from 1990 to 1996 by providing station overlaps in the transition from the original global tracking configuration to the current IGS network. However, our computations have shown that the same velocity field for PNG is generated without the additional data. This indicates that the PNG data set alone is sufficiently strong such that additional fiducial tracking data is not necessary to stabilize the velocity solution. Nonetheless, we have retained the additional data in the analysis as it allowed us to compute velocities of many additional sites on the Australian Plate and also to solve for plate motion vectors and relative poles between the Australian Plate and the microplates in PNG.

Appendix B: Reference Frames

Inherent in a GPS analysis for large-scale crustal deformation is a terrestrial reference frame, realized by the coordinates and velocities of tracking sites on the surface of the Earth. This becomes particularly important when combining data from many years in order to solve for site velocities. The definition of the terrestrial reference frame must be consistent and free of error in all of the data sets to be combined. If this is not the case, intercampaign biases will be introduced which will corrupt the site velocity estimates [see, e.g., *Larson et al.*, 1991].

A reference frame is fundamentally defined by an origin of a coordinate system, three orthogonal axes, and a scale. The realization of such a reference frame is via the three-dimensional coordinates of points on the surface of the Earth [*Lambeck*, 1988]. Hence different coordinate sets for the same points on the Earth effectively define different terrestrial reference frames. The International Terrestrial Reference Frame (ITRF) is an evolving reference frame whose accuracy is improving as new space geodetic measurements are added, and the differences between successive frames reflect the improvements in the accuracy of the frames rather than showing the time evolution of the coordinates. ITRF94 is a particular set of coordinates and velocities which refer to January 1, 1993, but can be transformed into another epoch by the addition of the velocity component. Many of the sites in the IGS global tracking GPS network have coordinates determined in ITRF94, and 13 of these sites are considered to be "core" or fundamental sites of the coordinate system (Figure 4 above). The coordinates and velocities of the core IGS sites have formal uncertainties of about 1-3 mm, and 1-3 mm yr^{-1} in ITRF94 and changes in coordinates between different ITRF reference frames are of the order of 5-10 mm. As in most aspects of GPS data analyses, the formal uncertainties are overly optimistic, but our tests on the terrestrial reference frame and its stability indicate that all 13 core stations have position uncertainties under 20 mm (1σ) with nine of these stations having uncertainties under 10 mm (1σ).

Table A1. Corrections to International GPS Service for Geodynamics Core Station Velocities Using ITRF94 Velocities and NNR1A a priori Velocities for the Core Stations

Site	Code	ITRF94-GPS		NNR1A-GPS	
		V_n	V_e	V_n	V_e
Algonquin, Canada	ALGO	-1.8	2.1	3.3	3.1
Fairbanks, Alaska	FAIR	-0.4	1.0	-1.6	2.2
Goldstone, United States	GOLD	-1.9	2.5	-1.5	2.0
Hartebeestoek, South Africa	HART	-0.7	-2.5	-1.3	-6.3
Kokee Park, Hawaii	KOKB	0.8	0.0	2.1	-1.8
Kootwijk, Netherlands	KOSG	0.1	0.4	1.1	1.8
Madrid, Spain	MADR	0.6	-1.3	-0.3	0.6
Santiago, Chile	SANT	-1.0	-0.6	-2.3	-0.5
Tidbinbilla, Australia	TIDB	2.5	-0.7	3.3	0.1
Tromso, Norway	TROM	0.4	0.4	3.5	0.6
Wettzell, Germany	WETT	2.1	4.6	2.3	6.0
Yaragadee, Australia	YAR1	-1.8	-1.3	-1.5	-2.2
Yellowknife, Canada	YELL	-0.5	0.3	-0.7	1.8
Mean		-0.1	0.4	0.5	0.6
Sigma of a single obs		1.4	1.9	2.2	3.0

Units are mm yr^{-1}.

The GAMIT and GLOBK processing procedure produces a free-network estimate of a polyhedron of global GPS sites that is only loosely oriented with respect to any terrestrial reference frame. The coordinates of this free network represent the locations of the sites with respect to each other, and the velocities show the deformation of the network as a result of tectonic motion. We aligned the free network with ITRF94 by computing seven-parameter Helmert transformations (three translations, three rotations, and one scale) on the coordinates and velocities of the 13 core IGS sites into ITRF94. The resulting scale factors are statistically insignificantly different from zero (1σ confidence interval), indicating that the scale of our network is consistent with the scale of the ITRF94 which is based on VLBI, SLR, and GPS data. In order to minimize unmodeled systematic effects in the antenna electrical phase center and residual atmospheric delay errors the height component was downweighted such that the transformation was based on the horizontal component of the solutions.

We tested the effect of using the older and less accurate reference frames (ITRF 92 and 93) by estimating the Helmert transformations for each of the three coordinate sets. The postfit root-mean-square (rms) of the coordinate transformations were 27, 15, and 5 mm for ITRF 92, 93, and 94, respectively, and the shape of our free global network clearly fits ITRF94 better than the earlier reference frames. The mean adjustments to ITRF94 velocities at the core IGS sites after the Helmert transformation are <1 mm yr^{-1}, with a 1σ standard deviation of a single observation of 1.4 mm yr^{-1} and 1.8 mm yr^{-1} for north and east, respectively (Table A1). This is within the quoted formal uncertainties of the ITRF94 core site velocities, and so, we can assume that our network is not significantly different from ITRF94.

We also computed the changes in the core station velocities using the ITRF94 values as a priori station coordinates and a priori velocities as predicted by the NNR1A plate motion model (Table A1). The mean corrections from this solution were <1 mm yr^{-1} but the actual estimates for the core station velocities returned to our original values; that is, the velocity estimates are independent of the a priori values used. The 1σ standard deviations increased to 2.2 mm yr^{-1} and 3.1 mm yr^{-1} for north and east, respectively. This indicates that there is a difference between the velocity field of ITRF94 and NNR1A, a difference which is larger than the uncertainties of the core station velocities. Our site velocities agree more closely with the velocities of ITRF94 than with the NNR1A velocities.

Acknowledgments. The GPS fieldwork conducted during 1990-1996 involved many institutions, both in PNG and Australia. Special thanks to the PNG National Mapping Bureau (NMB) for their considerable assistance in the form of equipment and personnel. GPS equipment was provided by Armar Larman Surveys, Australian Surveying and Land Information Group (AUSLIG), NMB, Centre for Remote and Environmental Studies at The Australian National University, the National Tidal Facility, Charles Sturt University, and The University of South Australia. We thank the Rabaul Volcanological Observatory and Department of Lands and Physical Planning at Rabaul for their assistance and participation in this project. R. Curley and the final year surveying students at The PNG University of Technology, Lae, assisted in the 1996 fieldwork. Also, we wish to express our gratitude to the many village people who assisted in the surveys. AUSLIG provided fiducial tracking data at many GPS sites in Australia. We thank the Scripps Orbit and Permanent Array Center for the use of global solutions for the 1996 analysis. Financial support for the field campaigns was provided by The PNG University of Technology, Lae, The Australian National University, The University of New South Wales, The University of Canberra, and the Australian Research Council . We thank C. DeMets, R. McCaffrey, and K. Hurst for helpful review comments. Maps and figures were generated using the Generic Map Tools (GMT) software version 3 [*Wessel and Smith*, 1995.]

References

Abbott, L. D., Neogene tectonic reconstruction of the Adelbert-Finisterre-New Britain collision, northern Papua New Guinea, *J. Southeast Asia Earth Sci., 11*, 33-51, 1995.

Abbott, L. D., E. A. Silver, P. R. Thompson, M. V. Filewicz, C. Schneider, and Abdoerrias, Stratigraphic constraints on the development and timing of arc-continent collision in northern Papua New Guinea, *J.* Sediment. *Res., Sect. B, 64*, 169-183, 1994.

Abers, G. A., and R. McCaffrey, Active arc-continent collision: Earthquakes, gravity anomalies, and fault kinematics in the Huon-Finisterre collision zone, Papua New Guinea, *Tectonics, 13*, 227-245, 1994.

Abers, G. A., and S. W. Roecker, Deep structure of an arc-continent collision: earthquake relocation and inversion for upper mantle P and S wave velocities beneath Papua New Guinea, *J. Geophys. Res., 96*, 6379-6401, 1991.

Argus, D. F., and M. B. Heflin, Plate motion and crustal deformation estimated with geodetic data from the Global Positioning System, *Geophys. Res. Lett., 22*, 15, 1973-1976, 1995.

Baldwin, S. L., G. S. Lister, J. E. Hill, D. A. Foster, and I. McDougall, Thermochronologic constraints on the tectonic evolution of active metamorphic core complexes, D'Entrecasteaux Islands, Papua New Guinea, *Tectonics, 12*, 611-628, 1993.

Benes, V., S. D. Scott, and R. A. Binns, Tectonics of rift propagation into a continental margin: Western Woodlark Basin, Papua New Guinea, *J. Geophys. Res., 99*, 4439-4455, 1994.

Beutler, G., I. Bauersima, W. Gurtner, M. Rothacher, and T. Schildknecht, Evaluation of the 1984 Alaska Global Positioning System campaign with the Bernese software, *J. Geophys. Res., 92*, 1295-1303, 1987.

Beutler, G., E. Brockman, W. Gurtner, U. Hugentobler, L. Mervant, M. Rothacher, and A. Verdun, Extended orbit modeling techniques at the CODE processing center of the international GPS service for geodynamics (IGS): Theory and initial results, *Manus. Geod., 19*, 367-386, 1994.

Beutler, G., E. Brockman, U. Hugentobler, L. Mervart, M. Rothacher, and R. Weber, Combining consecutive short arcs into long arcs for precise and efficient GPS orbit determinations, *J. Geod., 70*, 287-299, 1996.

Blewitt, G., Advances in Global Positioning System technology for geodynamics investigations: 1978-1992, in *Contributions of Space Geodesy to Geodynamics: Technology, Geodyn. Ser., vol. 25*, edited by D.E. Smith and D.L. Turcotte, pp. 195-213, AGU, Washington, D.C.,1993.

Bock, Y., P. Fang, K. Stark, J. Zhang, J. Genrich, S. Wdowinski, and S. Marquez, Scripps Orbit and Permanent Array Center: Report to '93 IGS Bern Workshop, in *Proceedings of the 1993 IGS Workshop, 25-26 March, 1993*, edited by G. Beutler and E. Brockman, pp. 101-110, Druckerei der Universität Bern, Bern, 1993.

Boucher, C., Z. Altamimi, M. Feissel, and P. Sillard, Results and analysis of the ITRF94, *Intern. Earth Rotation Serv. Tech. Note 20*, Observatoire de Paris, Paris, 1996.

Cooper, P., and B. Taylor, Seismotectonics of New Guinea: A model for arc reversal following arc-continent collision, *Tectonics, 6*, 53-67, 1987a.

Cooper, P., and B. Taylor, The spatial distribution of earthquakes, focal mechanisms, and subducted lithosphere in the Solomon Islands, in *Marine Geology, Geophysics and Geochemistry of the Woodlark Basin-Solomon Islands*, edited by B. Taylor and N. F. Exon, *Circum-Pac. Counc. Energy Miner. Resour. Earth Sci. Ser., 7*, 67-88, 1987b.

Curtis, J. W., Plate tectonics of Papua New Guinea - Solomon Islands region, *J. Geol. Soc. Aust., 20*, 21-36, 1973.

D'Addario, G. W., D. B. Dow, and R. Swodoba, Geology of Papua New Guinea scale 1:2,500,000. Bur. of Miner. Resour., Canberra, A.C.T., Australia, 1976.

Davies, H. L., P. A. Symonds, and I. Ripper, Structure and evolution of the Solomon Sea region, *BMR J. Aust. Geol. Geophys., 9*, 49-68, 1984.

Davies, H. L., E. Honza, D. L. Tiffin, J. Lock, Y. Okuda, J. B. Keene, F. Murakami, and K. Kisimoto, Regional setting and structure of the western Solomon Sea, *Geo. Mar. Lett., 7*, 153-160, 1987.

Davis, J. L., W. H. Prescott, J. L. Svarc, and K. J. Wendt, Assessment of Global Positioning System measurements for studies of crustal deformation, *J. Geophys. Res., 94,* 13,635-13,650, 1989.

DeMets, C., R. G. Gordon, D. F. Argus, and S. Stein, Current plate motions, *Geophys. J. Int., 101,* 425-478, 1990.

DeMets, C., R. G. Gordon, D. F. Argus, and S. Stein, Effect of recent revisions to the geomagnetic reversal time scale on estimates of current plate motions, *Geophys. Res. Lett., 21,* 2191-2194, 1994.

Denham, D., Distribution of earthquakes in the New Guinea-Solomon Islands region, *J. Geophys. Res., 74,* 4290-4299, 1969.

Dewey, J. F., and J. M. Bird, Mountain belts and the new global tectonics. *J. Geophys. Res., 75,* 2625-2647, 1970.

Eguchi, T., Y. Fujinava, M.Ukawa, and L. Bibot, Earthquakes associated with the back-arc opening in the eastern Bismarck Sea: Activity, mechanisms and tectonics, *Phys. Earth Planet. Inter., 56,* 189-209, 1989.

Eiichi, H., J. Keene, and D. L. Tittin, Plate boundaries in Solomon Sea region and subduction at trenches, *Am. Assoc. Petrol. Geol. Bull., 70,* 7, 927, 1986.

Engdahl, E. R., R. van der Hilst, and R. P. Biland, Global teleseismic earthquake relocations with improved travel times and procedures for depth determination, *Bull. Seismol. Soc. Am.*, in press, 1998.

Erlandson, D. L., T. L. Orwig, G. Kilsgaard, J. H. Mussells, and L. W. Kroenke, Tectonic interpretation of the East Caroline and Lyra basins from reflection profiling investigations, *Geol. Soc. Am. Bull., 87,* 453-462, 1976.

Feigl, K. L., et al., Space geodetic measurements of crustal deformation in central and southern California, 1984-1992, *J. Geophys. Res., 98,* 21,677-21,712, 1993.

Goodliffe, A. M., B. Taylor, F. Martinez, R. Hey, K. Maeda, and K. Ohno, Synchronous reorientation of the Woodlark Basin Spreading Center, *Earth Planet. Sci. Lett., 146,* 233-242, 1997.

Hamilton, W., Tectonics of the Indonesian region, *Bull. Geol. Soc. Malays., 6,* 3-10, 1973.

Hamilton, W., Tectonics of the Indonesian region, *U.S. Geol. Surv. Prof.* Paper *1078,* 354pp, 1979.

Hegarty, K. A., J. K. Weissel, and D. E. Hayes, Convergence of the Caroline and Pacific Plates: Collision and subduction, in *The Tectonic and Geologic Evolution of the Southeast Asian Sea and Islands, Part 2, Geophys. Monogr. Ser.*, edited by D. E. Hayes, vol. 27, pp. 326-348, AGU, Washington, D.C., 1983.

Herring, T. A., J. L. Davis, and I. I. Shapiro, Geodesy by radio interferometry: The application of Kalman filtering to the analysis of very long baseline interferometry data, *J. Geophys. Res., 95,* 12,561-12,581, 1990.

Hudnut, K. W., et al., Co-seismic displacements of the 1994 Northridge, California, earthquake, *Bull. Seismol. Soc. Am,* 86, s19-s36, 1996.

Johnson, R. W., Geotectonics and volcanism in Papua New Guinea: a review of the late Cainozoic, *BMR J. Aust. Geol. Geophys., 4,* 181-207, 1979.

Johnson, R. W., and A. Jaques, Continent-arc collision and reversal of arc polarity: New interpretations from a critical area, *Tectonophysics, 63,* 111-124, 1980.

Johnson, T., and P. Molnar, Focal mechanisms and plate tectonics of the southwest Pacific, *J. Geophys. Res., 77,* 5000-5032, 1972.

Karig, D. E., Remnant arcs, *Geol. Soc. Am. -Bull., 83,* 1057-1068, 1972.

King, R. W., and Y. Bock, Documentation for the GAMIT GPS analysis software, *Release 9.6,* Mass. Inst. of Technol., Cambridge, 1996.

Kirchoff-Stein, K. S., Seismic reflection study of the New Britain and Trobriand subduction systems and their zone of initial contact in the western Solomon Sea, Ph.D. thesis, 248 pp., Univ. of Calif., Santa Cruz, 1992.

Krause, D. C., Crustal plates of the Bismarck and Solomon Seas, in *Oceanography of the South Pacific 1972,* edited by R. Fraser, pp. 271-280, New Zealand Natl. Comm., UNESCO, Wellington, 1973.

Lambeck, K., Geophysical geodesy: The slow deformation of the Earth, 718 pp., *Oxford Univ. Press,* Oxford, New York, 1988.

Larson, K. M., F. W. Webb, and D. C. Agnew, Application of the Global Positioning System to crustal deformation measurement, 2, The influence of errors in Orbit Determination Networks, *J. Geophys. Res., 96,* 16,567-16,589, 1991.

Larson, K. M., J. Freymueller, and S. Philipsen, Global plate velocities from the Global Positioning System, *J. Geophys. Res., 102,* 9961-9981, 1997.

Lichten, S. J. and J. S. Border, Strategies for high precision GPS orbit determination, *J. Geophys. Res., 92,* 12,751-12,762, 1987.

Lock, J., H. L. Davies, D. L. Tiffin, F. Murakami, and K. Kisimoto, The Trobriand subduction system in the western Solomon Sea, *Geo. Mar. Lett., 7,* 129-134, 1987.

Martinez, F., and B. Taylor, Manus Basin, Bismarck Sea: An epitome of microplate deformation, *Eos Trans. AGU, 73* (43), Fall Meet. Suppl., 605, 1993.

McCaffrey, R., Slip partitioning at convergent plate boundaries of SE Asia, in *Tectonic Evolution of Southeast Asia,* edited by R. Hall, and D. Blundell, *Geol. Soc. Spec. Pub, 106,* 3-18, 1996.

McClusky, S., K. Mobbs, A. Stolz, D. Barsby, W. Loratung, K. Lambeck, and P. Morgan, The Papua New Guinea satellite crustal motion surveys, *Aust. Surv., 39,* 194-214, 1994.

McKee, C., B. Talai, N. Lauer, R. Stewart, P. deSaint Ours, I. Itikari, H. Patia, D. Lolok, H. Davies, and R. W. Johnson, The 1994 eruption at Rabaul volcano, Papua New Guinea, paper presented at General Assembly, Int. Union of Geod. and Geophys., Boulder, CO, 1995.

Mobbs, K., Tectonic interpretation of the Papua New Guinea region from repeat satellite measurements, *Unisurv Rep., S-48,* 256 pp, Univ. of N.S.W., Kensington, N.S.W., Aust., 1997.

Morgan, P. J., National baseline sea-level monitoring program, final report, 86 pp., Fac. of Inf. Sci. and Eng., *Univ. of Canberra,* Canberra, A.C.T., Aust., 1994.

Mori, J., The New Ireland earthquake of July 3, 1985, and associated seismicity near the Pacific-Solomon Sea-Bismarck Sea triple junction, *Phys. Earth Planet. Int., 55,* 144-153, 1989.

Mueller, I. I., and G. Beutler, The International GPS Service for Geodynamics - Development and Current Status, paper presented at the Sixth International Geodetic Symposium on Satellite Positioning, Columbus, Ohio, March, 1992.

Pegler, G., S. Das, and J. H. Woodhouse, A seismological study of the eastern New Guinea and the western Solomon Sea regions and its tectonic implications, *Geophys. J. Int., 122,* 961-981, 1995.

Ripper, I. D., Seismicity of the Indo-Australian/Solomon Sea plate boundary in the southeast Papua region, *Tectonophysics, 87,* 355-369, 1982.

Robbins, J. W., D. E. Smith, and C. Ma, Horizontal crustal deformation and large scale plate motions inferred from space geodetic techniques, in *Contributions of Space Geodesy to Geodynamics: Crustal Dynamics, Geodyn. Ser.*, vol. 23, edited by D.E. Smith and L. Turcotte, pp. 21-36, AGU, Washington, D.C., 1993.

Ryan, H. F. and M. S. Marlow, Multichannel seismic-reflection data collected at the intersection of the Mussau and Manus trenches, Papua New Guinea, in *Geology and Offshore Resources of Pacific Island Arcs - New Ireland and Manus Region, Papua New Guinea,* edited by M. S. Marlow, S. V. Dadisman, and N. F. Exon, *Circum-Pac. Counc. Energy Miner. Resour. Earth Sci. Ser., 9,* 201-208, 1988.

Sloane, B. J., and J. B. Steed, Crustal movement survey, Markham Valley - Papua New Guinea, *Tech. Rep., 23,* Dep. of Natl. Resour., Div. of Natl. Mapp, Canberra, A.C.T., Aust., 1976.

Smith, I. E., Peralkaline rhyolites from the D'Entrecasteaux Islands, Papua New Guinea, in *Volcanism in Australasia,* edited by R. W. Johnson, pp. 275-285, Elsevier, New York, 1976.

Taylor, B., The tectonics of the Bismarck Sea region, *B. Sc thesis,* Univ. of Sydney, Sydney, N.S.W., Aust., 1975.

Taylor, B., The Bismarck Sea: Evolution of a back-arc basin, *Geology, 7,* 171-174, 1979.

Taylor, B., A geophysical survey of the Woodlark-Solomons region, in *Marine Geology, Geophysics and Geochemistry of the Woodlark Basin-Solomon Islands,* edited by B. Taylor and N. F. Exon, *Circum-Pac. Counc. Energy Miner. Resour. Earth Sci. Ser., 7,* 25-48, 1987.

Taylor, B. and N. F.Exon, An investigation of ridge subduction in the Woodlark-Solomons region: Introduction and overview, in *Marine Geology, Geophysics and Geochemistry of the Woodlark Basin-Solomon Islands,* edited by B. Taylor and N. F. Exon, *Circum-Pac. Counc. Energy Miner. Resour. Earth Sci. Ser., 7,* Houston, Tex., 1-24, 1987.

Taylor, B., K. A. W., Crook, J. M. Sinton, L.Petersen, R.Mallonee, J.N. Kellogg, and F. Martinez, Manus Basin, Papua New Guinea, SeaMARC II sidescan sonar imagery, bathymetry, magnetic anomalies, and free air gravity anomalies, *Pacific Seafloor Atlas,* Sheet 7, scale 1: 1,000,000, Hawaii Inst. Geophys., Honolulu, 1991.

Taylor, B., A. Goodliffe, F. Martinez, and R. Hey, Continental rifting and initial sea-floor spreading in the Woodlark basin, *Nature, 374,* 534-537, 1995.

Tregoning, P., GPS measurements in the Australian and Indonesian

regions (1989-1993), *Unisurv Rep., S-44*, 134 pp, Univ. of N. S. W., Kensington, N.S.W., Aust., 1996.

Tregoning, P., F. K. Brunner, Y. Bock, S. S. O. Puntodewo, J. F.Genrich, E.Calais, J.Rais, and C. Subarya, First geodetic measurement of convergence across the Java Trench, *Geophys. Res. Lett., 21*, 2135-2138, 1994.

Weissel, J. K., and R. N. Anderson, Is there a Caroline plate?, *Earth Planet. Sci. Lett., 41*, 143-158, 1978.

Weissel, J. K., B. Taylor, and G. D. Karner, The opening of the Woodlark Basin, subduction of the Woodlark spreading system and the evolution of northern Melanesia since mid-Pliocene times, *Tectonophysics, 87*, 253-277, 1982.

Wessel, P. and W.H.F. Smith, New version of the generic mapping tools released, *Eos Trans. AGU, 76* (33), 329, 1995.

R. J. Jackson and R. P. Little, Department of Surveying and Land Studies, Papua New Guinea University of Technology, Private Mail Bag, Lae, Morobe Province, Papua New Guinea. (e-mail: rjackson@survey.unitech.ac.pg)

K. Lambeck, H. McQueen, P. Tregoning, and P. van der Beek, Research School of Earth Sciences, The Australian National University, Canberra, A.C.T. 0200, Australia (e-mail: pault@rses.anu.edu.au)

S. C. McClusky, Department of Earth, Atmospheric and Planetary Sciences, Massachusetts Institute of Technology, 77 Massachusetts Avenue, Cambridge, MA 02139. (e-mail: simon@chandler.mit.edu)

P. J. Morgan, School of Information Science and Engineering, University of Canberra, P.O. Box 1, Belconnen, A.C.T. 2601, Australia. (e-mail: peterm@bomford.canberra.edu.au)

B. Murphy, Australian Surveying and Land Information Group, Fern Hill Park, Bruce, A.C.T. 2601, Australia. (e-mail: BrianMurphy@auslig.gov.au)

A. Stolz, School of Geomatic Engineering, The University of New Wales, Sydney, New South Wales 2052, Australia. (e-mail: A.Stolz@unsw.edu.au)

(Received June 26, 1997; revised November 23, 1997;
accepted December 15, 1997.)